Ricerca Sistema Elettrico	Sigla di identificazione	Distrib.	Pag.	di
	ADPFISS – LP2 – 085	L	1	89

Titolo

Characterization of the new ALFRED core configuration

Descrittori

Tipologia del documento: Rapporto Tecnico
Collocazione contrattuale: Accordo di programma ENEA-MSE su sicurezza nucleare e reattori di IV generazione
Argomenti trattati: Reattori veloci
Progetto Nocciolo

Sommario

Dopo l'attività di revisione critica del progetto di nocciolo di ALFRED e l'individuazione di soluzioni atte a superare le criticità, effettuate nell'ambito del precedente piano annuale di realizzazione, si è provveduto a integrare ed armonizzare tutte le soluzioni in una nuova configurazione di nocciolo, quindi a caratterizzare quest'ultima da un punto di vista neutronico.
I risultati così ottenuti sono quindi stati utilizzati per una successiva fase preliminare di verifica, evidenziando come la nuova configurazione, rispettando tutti i vincoli termoidraulici e di stabilità dinamica, possa essere assunta come nuovo riferimento per il nocciolo di ALFRED.

Note:

Riferimento CIRTEN: **CERSE-POLIMI RL 1602/2015**

Autori: F. Lodi[2], G. Grasso[1], A. Cammi[3], S. Lorenzi[3], C. Petrovich[1], D. Mattioli[1], M. Sumini[2]

(1) ENEA
(2) Università di Bologna
(3) Politecnico di Milano

Copia n. **In carico a:**

2			NOME			
			FIRMA			
1			NOME			
			FIRMA			
0	EMISSIONE	28/09/15	NOME	G. Grasso	M. Tarantino	M. Tarantino
			FIRMA			
REV.	DESCRIZIONE	DATA		REDAZIONE	CONVALIDA	APPROVAZIONE

Table of Contents

Acronyms and Abbreviations 3

1. Introduction 4

2. Summary of the critical review of the previous configuration 4

3. New reactor models 5

4. Characterization of the new core configuration 6

4.1. Investigation of ALFRED stability and dynamics 9

4.1.1. Stand-alone core analysis 9

4.1.2. Primary loop analysis 11

5. Steady state thermal-hydraulic verification 14

6. Conclusions 16

References 17

Appendix - Simulation tools for the assessment of the stability and the dynamics of the new ALFRED configuration 18

A.1. Model development 18

A.1.1. Neutronics 18

A.1.2. Thermal-hydraulics 18

A.1.3. Reactivity 19

A.1.4. Primary loop 19

A.2. Method 20

Acronyms and Abbreviations

ADF – Axial Distribution Factor

ALFRED – Advance Lead Fast REactor European Demonstrator

BoC – Beginnning of Cycle

BoL – Beginning of Life

CR – Control Rod

DPA – Displacement Per Atom

EoC – End of Cycle

FA – Fuel Assembly

FADF – Fuel Assembly Distribution Factor

FPDF – Fuel Pin Distribution Factor

GIF – Generation IV International Forum

INN – Inner Fuel

LEADER – Lead-Cooled European Advance DEmonstration Reactor

OUT – Outer Fuel

1. Introduction

ALFRED – Advanced Lead Fast Reactor European Demonstrator – is the first nuclear reactor whose design has been entirely conceived and developed by an international community of researchers, taking inspiration from the ambitious concept expressed by the Generation IV International Forum (GIF) [1] for a new generation of nuclear energy systems more safe, clean, economical and proliferation resistant. Identified in the innovative technology of heavy liquid metals the more promising solution to reach the above mentioned objectives, ALFRED will have the double role of showing the idea's validity, proving its technical feasibility, but also to quantitatively demonstrate the possibility of reaching degrees of safety, sustainability and economic competitiveness that will allow, to this new kind of reactors, meeting the population requests towards a sustainable and secure future [2-4].

In line with this vision, the present technical report is a continuation of the national and international studies and researches for the further development of the reactor design, with particular emphasis on the core design, in order to put to fruition the last two years of the Programmatic Agreement (Accordo di Programma) and finally establishing a new reference configuration for the ALFRED core. In particular, after the detailed analysis of the core configuration, as emerged from the LEADER project, in the last year we arrived at a possible arrangement in which all the revealed criticalities have been corrected [5]. The major aim of the activity of this year is the complete neutronic characterization, so as to retrieve enrichments and enrichment zoning which will allow to guarantee the operability of the reactor for the foreseen time span, respecting all the design constraints. The data obtained from this characterization will then be used to verify the assembly thermal-hydraulics and the pin thermo-mechanics, so as to cross-check the achievement of the aforementioned objectives. Since some modifications are expected also to impact on the reactivity coefficients, a model for the analysis of ALFRED dynamics will be developed, and applied to investigate the stability of the system.

2. Summary of the critical review of the previous configuration

In the last year of the Programmatic Agreement various critical points of the previous core configuration (Figure 1) were analyzed and appropriate solutions proposed, critically discussed and – where possible – tested estimating their impact on the design parameter they were directly acting upon. In a brief survey the proposed solutions were:

1) Enlargement of the wrapper inner key so to prevent overheating of the corner sub-channels. Combining this with the need to replace the original wrapper material, and having identified the 15-15Ti austenitic stainless steel as candidate, it was decided to reduce the thickness of the hexcan – taking profit of the superior mechanical performances of the latter with respect to T91 – in order to limit the impact on criticality.

2) A multifunctional shield with different elements in the different regions surrounding the multiplicative zone so to protect the inner vessel from excessive neutronic damage. The shield is composed of a reflecting region close to the core, and an absorbing region near the inner vessel.

3) In order to have more realistic simulations, in all the reactor models pure lead was substituted with one at a commercially available purity. The standard brand C1 was identified as the less expensive, still ensuring manageable polonium production.

4) Given the nature of demonstrator, it was considered to introduce within the core region as many locations for instrumentation as possible, to allow for a comprehensive acquisition of data on the neutronic performances of the system.

These solutions and modeling choices, applied to the existing ALFRED configuration from the LEADER project, form the new reference configuration to be optimized and characterized.

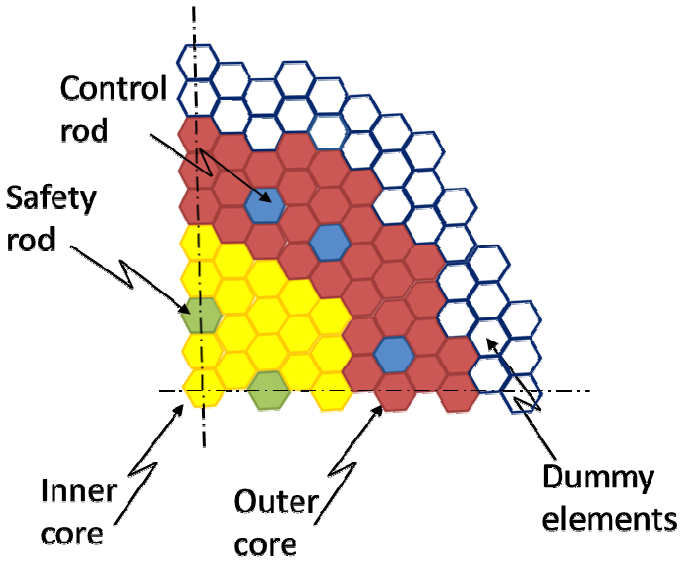

Figure 1 - ALFRED core layout (one quarter), LEADER version.

3. New reactor models

Given the necessity of characterizing a new configuration so as to establish the reference core of ALFRED and given the material and geometrical modifications to be added to the model, it seems appropriate to update the ERANOS and MCNP input; moreover, considering that the previous input decks for the two codes were prepared by different organizations (specifically CEA for ERANOS 2.2 and ENEA for MCNP 6.1), some inconsistencies were present in the material properties or temperatures used. Moreover, the inputs were prepared under the LEADER and previous AdP projects thus not taking into account the new modifications object of the last year. In light of these considerations a coherent set of physical properties has been chosen – based on a literature review – and adopted for both codes; the temperatures of the various components of the reactor have been equalized and thermal dilatation has been calculated so as to be as much as possible realistic and consistent among the codes. A series of checks has also been performed in order to guarantee that the main masses and volumes were effectively equal between ERANOS 2.2 and MCNP 6.1, and now it can be stated that the main discrepancies in results are due to the different numerical approach of the codes and to the used cross section library sets; to prove this statement in Table 1 are reported the keff calculated by the codes along with the errors on the radial power map. It is worth mentioning that differences as low as 70 pcm (for criticality) and 1.3% (for power distribution) between ERANOS and MCNP results indicates the high coherence achieved in the development of the two models.

Table 1 – Codes consistency comparison.

Code	ERANOS 2.2	MCNP 6.1	
Library	JEFF3.1	JEFF3.1.2	ENDF/B-7.1b
k_{eff}	1.08307	1.08373±21pcm	1.07756±22pcm
Max error on FA power at BoL (relative to MCNP-ENDF/B-7.1b)	1.32%	1.35%	--

A note on the library set to be used in MCNP 6.1 must be made: the European reference library set is the JEFF-3.2 which however, in our tests, revealed problems in running coupled neutron and gamma calculations which are deemed essential in order to have the photonuclear contribution to the criticality and the power deposition in non fissile regions like the coolant, cladding etc. For this reason they cannot be used. In order not to use the previous (oldest) release JEFF-3.1.2 the choice has been directed towards the US ENDF/B-7.1b; this is justified because in runs with only neutron transport the JEFF-3.2 and ENDF/B-7.1b are very close to each other while the JEFF-3.1.2 predicts higher values for the k_{eff} as visible in Table 2.

Table 2 – MCNP 6.1 library confrontation for neutron only transport calculations.

Library	JEFF-3.1.2	JEFF-3.2	ENDF/B-7.1b
k_{eff}	1.08367±21 pcm	1.07757±21 pcm	1.07767±20 pcm

Now that a common base for the codes has been settled, the core design can start; the results which will be show from now on are MCNP 6.1 results, but as stated, ERANOS 2.2 are very close and for the purpose of the neutronic design they can be effectively taken as equal.

4. Characterization of the new core configuration

The core design approach is an harmonization of thermal-hydraulic, mechanic and neutronic constraints in order to achieve certain goals, mainly related to safety, sustainability and economy. In the present study this approach will not be pursued since its very beginning because the fuel pin and assembly configuration are borrowed from the ALFRED core – LEADER version – plus the modifications previously discussed. The design will therefore be more oriented to the neutronic side in order to determine the new enrichments and enrichment zoning which will allow to guarantee the operability of the reactor for the foreseen time span, respecting all the constraints on the maximum cladding temperature and neutron damage on the reactor inner vessel internals (all constraints are borrowed from [3], but the main ones will be recalled in the present report).

One of the main limits to be respected is the 550°C on the cladding surface so to keep corrosion by liquid lead within acceptable levels; this must be respected throughout the whole core cycle in normal operation. The adopted neutronic design strategy is therefore to flatten as much as possible the clad temperature at pin level taking into account uncertainties from the

very beginning; this flattening is pursued at both EoC – End of Cycle – and BoC – Beginning of Cycle.

At EoC, coherently with the aim of maximizing fuel exploitation, the Control Rods (CR) are considered fully extracted, while at BoC they are inserted so as to compensate the reactivity excess required as reserve because of the burn-up swing. It then follows that the CRs are gradually withdrawn to compensate the fuel depletion and exactly at EoC they come in fully extracted position; this implies that on average the CRs are inserted halfway, or better, they are inserted so to give an anti-reactivity which is half the burn-up swing they are requested to compensate. Since the effect of the CRs is crucial at BoC, when it shifts the power distribution towards the core center and the upper portion of the active region (remembering that control rods in ALFRED are inserted from below), it is deemed necessary to take into account their effect. It must be said, however, that performing calculation with CRs movement is very difficult, sometimes lengthy if not even impossible (depending on the code). In the present work therefore a novel approach has been followed, which needs verification with direct calculation of the CR movements, enabling a realistic power map evaluation even without performing real CR movements during the burn-up simulations; the idea is to burn the core with the CR inserted halfway and evaluating the effect of their movement at BoC and EoC with calculations on a fresh core (BoL), with CRs fully inserted and fully extracted respectively. Through this it has been possible, by comparison with the half inserted calculation, to retrieve the correction factors to be applied to the Fuel Assemblies (FA), axial and pin-by-pin distributions factors. The factors calculated at BoL are applied at BoC and EoC assuming that the relative effect has been negligibly modified by the burnup; this is reasonable because the burnup swing is not very high and a relative effect such as this should be less sensitive than absolute effects, which are already small for the CRs in ALFRED. The calculated factor are reported in Table 3 where the two Axial Distribution Factors (ADF) correspond to the average value and the value for the end of the active length where the maximum cladding temperatures are located. Being the CRs inserted from below, it is important to account for their presence because they enhance power the top region of the core, where temperatures are indeed higher.

Table 3 – CRs insertion effect factors where FADF (FA Distribution Factor), ADF (Axial Distribution Factor) and FPDF (Fuel Pin Distribution Factor).

State	BoC		EoC	
Region	INN	OUT	INN	OUT
FADF	1.093	0.994	0.932	1.006
ADF_average	1.003	1.020	0.992	0.974
ADF_end core	0.988	1.047	0.969	0.922
FPDF	1.011	1.024	1.009	0.979

The enrichment zoning has been left unchanged from the previous configuration, only their ratio and absolute value has been modified. In order to respect the constraint on the maximum linear power achievable (340÷350 W/cm) the active length has been slightly increased, passing from 60 to 65 cm, keeping fixed the number of pins in the core. This also permits to respect the maximum Burn-Up limit so as to not incur in excessive Pellet-Clad Mechanical

Interactions which was fixed at some 100 MWd/kg. After an adjustment procedure so to flatten as much as possible the maximum cladding temperature, and so balancing the high power in the central FA and the high gradient in the outer FA, the new enrichments have been found to be: 22.2 wt.% and 27.4 wt.% for the inner and outer zone respectively; the reactivity evolution during time is reported in Figure 2, where is visible the about unity k_{eff} at EoC and a burnup swing of 2440 pcm. The maximum FA power at BoC and EoC (already corrected for the CRs effect), along with the maximum linear power are reported in Table 4; it is seen that the constraint is actually respected even considering an increase of some 3-4% to account for the refueling effect not consider in the 1-batch approximation.

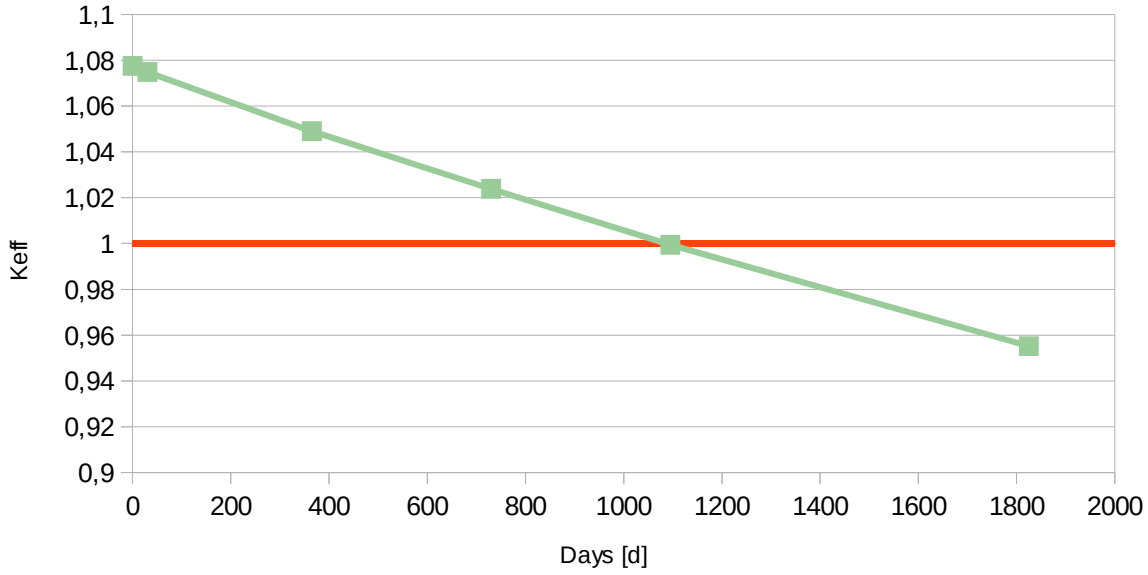

Figure 2 – k_{eff} evolution during burn-up.

Table 4 – Maximum power of the proposed configuration.

State	BoC		EoC	
Region	INN	OUT	INN	OUT
Max FA power [MW]	2.43	2.11	2.06	2.11
Max linear power [W/cm]	332	326	299	298

The average DPA calculated for the cladding in the active region for the peak flux pin are around 83 which, when multiplied by the axial distribution factor, becomes 95 thus respecting the 100 design constraint. The peak vessel DPA after 60 years is around 2 equaling the design limit; if necessary, the value can be further reduced by extending the height of the absorber portion of the Absorber Dummy Element close to the vessel by some 30 cm above the active region.

It must be pointed out that the increased height will worsen the coolant density effect in the core region and due to the increased pressure drops (partially compensated by the larger

wrapper inner key) will reduce the natural convection mass flow. Although the extent of these effects is not expected to pose concerns, thanks to the extreme safety margins of the original configuration [4] even in unprotected conditions, safety analysis are deemed necessary to confirm the performances of this option. Specifically referencing the increase of the coolant density effect, a dynamics analysis of ALFRED was performed to infer the stability of the system as a function of the associated reactivity coefficient.

4.1. Investigation of ALFRED stability and dynamics

Six different conditions have been considered to draw the poles of the system. In the first place, a stand-alone core configuration has been studied, in this case the inlet temperature is considered as a fixed input. In this condition, three major cases have been analyzed:

a) power level ranging between zero power and full nominal power at BoC;

b) power level ranging between zero power and full nominal power at EoC;

c) parametric variation of the lead density reactivity coefficient on the entire power range at BoC.

In the second place, the simplified primary system configuration has been taken into account, and the effects of closing the loop on stability have been assessed. Similarly to the stand-alone core study, three cases have been considered:

a) power level ranging between zero power and full nominal power at BoC with SG at nominal conditions;

b) power level ranging between zero power and full nominal power at BoC with SG at ideal heat exchange conditions;

c) parametric variation of the lead density reactivity coefficient on the entire power range at BoC with SG at nominal conditions.

4.1.1. Stand-alone core analysis

A stand-alone core analysis has been carried out aimed at verifying the core system stability in nominal conditions at different power levels at BoC. In particular, the neutronics block has been treated as the open loop, whereas the thermal-hydraulics with its reactivity coefficients constitutes the feedback loop, as depicted in Figure 3.

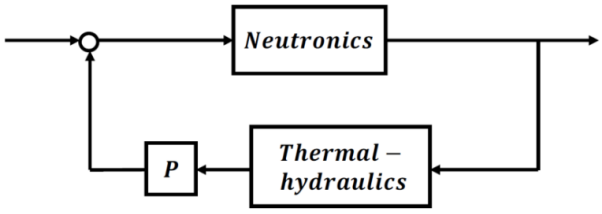

Figure 3 – conceptual feedback scheme employed to describe the stand-alone core behavior.

A thirteenth order system has been obtained by implementing the equations associated to the model described in Appendix A. After simplification and linearization, a four roots system

has been found: actually neutron precursors groups have been collapsed into a single one, and the cladding contribution has been simply neglected.

All the system roots lay on the left hand side of the Gauss plane, confirming that the core is stable on the entire power range (Poles at -4700 rad/s and -2.5 rad/s are not shown and discussed in this analysis since they do not change their position significantly with varying power and lead coefficient, resulting in an almost constant contribution to the system behavior).

More in detail, the neutronics-related pole is located in the origin when the reactor is at zero power conditions, and moves to the left as the power rises, due to the increasing effect of the temperature-induced negative reactivity feedbacks. At a certain power level the dominant poles become complex conjugated, as shown in Figure 4, indicating that power fluctuations occur. In particular, the imaginary part of the poles increases along with the rising power level, meaning that the frequency of the oscillations increases too. Despite the rise of the imaginary part of the poles, the magnitude of the real negative part grants the damping of such oscillations. This phenomenon ensues from the fact that in the linearized model the gain of the thermal feedback is proportional to the power level; thus, for equal variations of reactivity, the oscillation frequency grows as the power increases.

An analogous behavior is found at EoC, whose root locus is shown on the right side of Figure 4: the core exhibits the same stability characteristics as at BoC, coherently with the very slight differences between the respective reactivity coefficients and kinetic parameters. As a consequence of such minor discrepancies, it can be concluded that the influence of the fuel burn-up is definitely negligible as far as the system stability is concerned.

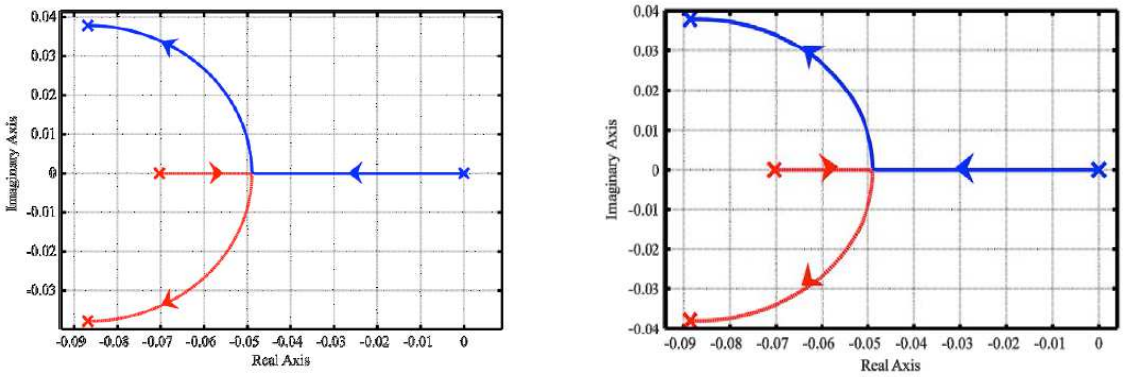

Figure 4 – root locus detailed view for the stand-alone core as a function of power level at BoC (left) and EoC (right).

The core system stability has been investigated also when making the coolant density reactivity coefficient parametrically vary from its positive nominal value to large positive figures, so as to determine a critical threshold rendering the system unstable.

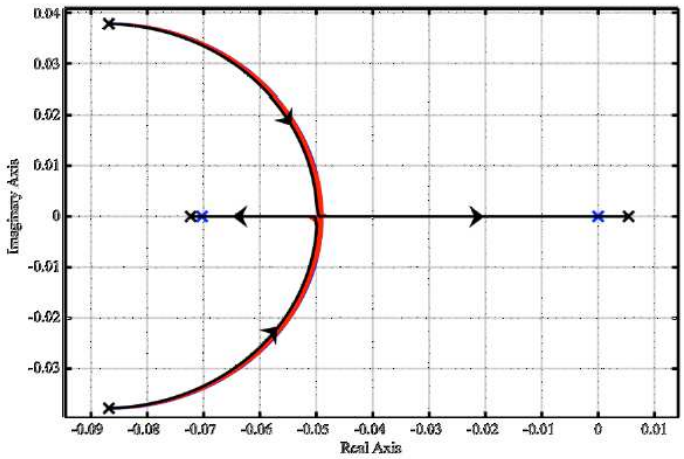

Figure 5 – root locus for the stand-alone core as a function of power level with the coolant density coefficient ranging from 0 to 12 pcm/K at BoC.

As shown in Figure 5, the blue track represents the poles trajectory as a function of power level (from 0 to 300 MWth) with the coolant density coefficient kept constant at its nominal value. The red lines represent the poles trajectories evaluated at discrete power levels (from 30 MWth to nominal power, with 10% steps) as a function of the coolant density coefficient varying from 0 to 12 pcm/K. In this latter case, for increasing values of the lead density coefficient, the roots move to the right, becoming first real and then also positive at a certain critical value around 12 pcm/K. Such a trend is not always the same since the critical value depends on the power level considered: actually, the system at nominal power becomes unstable for the lowest lead density coefficient (as described in Figure 5, black track). This trend is mainly due to the amplified feedback effects at higher power. In fact, if the action of a feedback is destabilizing (i.e., the corresponding reactivity coefficient is positive), its impact is first noticed at high power, where its magnitude is larger because more amplified. In addition, the (negative, that is stabilizing) Doppler effect is stronger at low power levels, and decreases along with the power level increase. Therefore, at low power levels there is a stronger counteraction by the Doppler effect, which counterbalances the lead density coefficient positive action. In other words, the core behavior is more sensitive to this design parameter variation at nominal power, and thus it may be concluded that, at low power levels, the system is more robust to uncertainties affecting its value. In any case, it has been seen that the system becomes unstable only for extremely high values of the coolant density coefficient, a clearly non-realistic condition.

Therefore, it can be stated that the system is inherently stable, and consequently safe, both at low power levels and in the case of positive coolant density reactivity coefficients.

4.1.2. Primary loop analysis

A stability analysis has been carried out also in a primary loop configuration in order to consider a more realistic situation in which the SG feedback action on the core dynamics is taken into account (Figure 6).

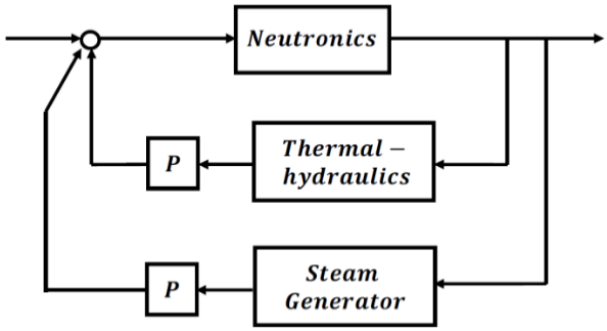

Figure 6 – conceptual feedback scheme employed to describe the primary loop behavior.

Equations representing the influence of the SG and the closure of the primary loop (see Appendix A) have been added to the previous set of equations, obtaining a total of sixteen equations. Also in this case, model simplification and linearization have reduced the dimension of the equation set: finally, a seven roots system has been considered.

As Figure 7 illustrates, the system is still stable in nominal conditions at each power level, but compared to the previous case, additional complex conjugate poles appear in the plots: a new dynamics has been found on the right of the trajectories representing the stand-alone core; the new tracks are closer to the origin and complex conjugate for low power levels, suggesting that the dynamics they describe is slower and with damped oscillations In this case only one pole remains close to the origin also at high power levels, whereas in the stand-alone core analysis both the roots move to the left. As mentioned previously, when coupling the core with the SG the coolant core inlet temperature is no longer a fixed input, becoming instead a state variable depending on the power exchange conditions at the interface with the secondary side. This induces a feedback on the core behavior, whose neutronics is influenced by the reactivity effects led by temperature changes.

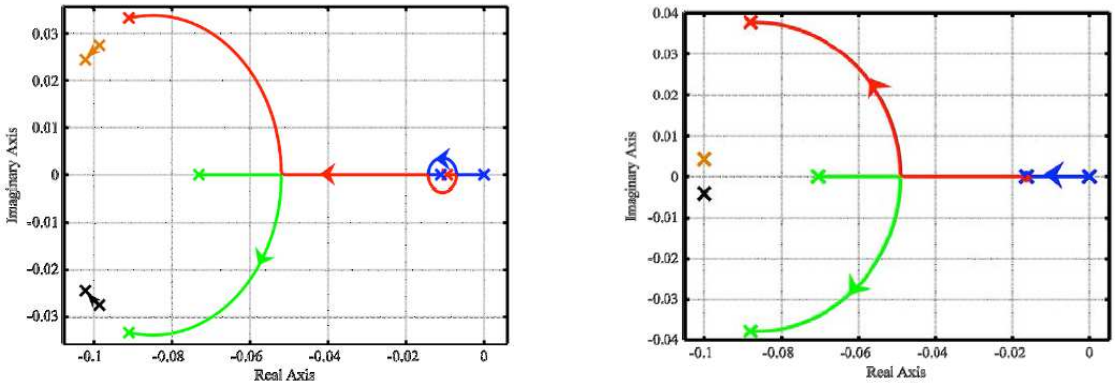

Figure 7 – root locus for the primary system as a function of power level at BoC, in nominal SG conditions (left) and ideal exchange conditions (right).

When the SG is set at nominal conditions, any power variation on the core side causes the core inlet temperature to change affecting the system reactivity (primarily due to the coolant temperature variation, with a consequent additional lead density and radial expansion feedback), differently than in the stand-alone core case, in which the inlet temperature is a fixed input. Such phenomena explain the system new oscillatory behavior at low power shown in Figure 7.

In addition, the situation of ideal heat exchange conditions on the SG side have been considered (Figure 7, right graph): it clearly appears how, for increasing exchange capabilities, the circle moves to the left and reduces its dimensions, meaning that oscillations progressively damp as the stand-alone core case is asymptotically approached (i.e. inlet temperature independent of the SG heat exchange capabilities). In both the above mentioned situations, the primary loop pole trajectories have been examined again as a function of the lead density coefficient variation (Figure 8).

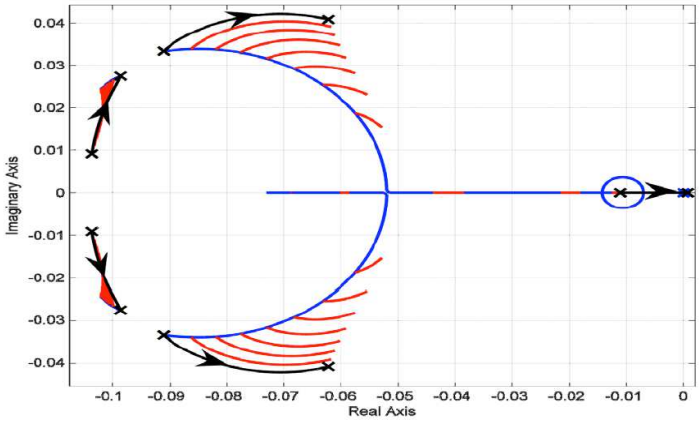

Figure 8 – root locus for the primary system as a function of power level with lead density coefficient ranging between 0 and 7 pcm/K at BoC, in nominal SG conditions.

As in the previous graphs, the blue track constitutes the roots trajectories when the power varies and the lead density coefficient is equal to its nominal value, whereas red tracks represent the poles motion induced by variations of the lead density coefficient from 0 to 7 pcm/K at each power level (the nominal power is depicted with black track).

By comparing Figure 8 with Figure 5,it can be inferred that the primary loop system behaves qualitatively as the stand-alone core one, but the instability threshold is reached earlier in the former case: for increasing values of the lead density coefficient the poles move to the right and become real positive when the coolant density coefficient is between 6 and 7 pcm/K, evidencing a kind of “destabilizing” action by the SG.

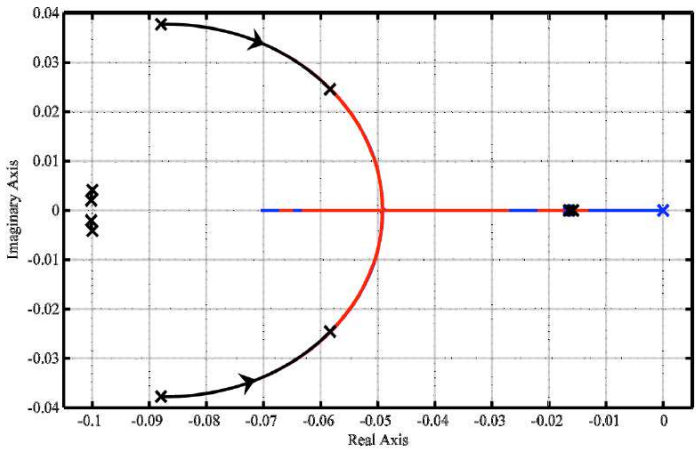

Figure 9 – root locus for the primary system as a function of power level with lead density coefficient ranging between 0 and 7 pcm/K at BoC, in ideal perfect exchange conditions.

In confirmation of this, the system stability has been analyzed by connecting a progressively more performing SG to the core, and it appears very clearly that the closer the heat exchange conditions are to the ideal ones, the higher is the margin of stability of the reactor system, since the core is less and less influenced by the secondary side dynamics. Indeed, when considering an ideal SG (Figure 9), the poles never reach a positive real part for the considered range of the lead density coefficient, implying that greater values of the reactivity coefficient are needed for the system to become unstable, likewise in the only core case (Figure 5).

Anyway, even when considering the closed system configuration with nominal SG conditions, the reactor becomes unstable only for very high values of the lead density coefficient, which are still non-realistic. Therefore, it can be definitely concluded that the overall system is indeed inherently stable, and consequently safe.

5. Steady state thermal-hydraulic verification

In order to check the consistency of the adopted design methodology and to ensure that the temperature constraints are effectively met under steady state conditions, a detailed analysis at FA level is necessary. The numerical method selected for this purpose is the sub-channel one by means of the ANTEO+ code [6]. In order to have simulations as realistic as possible, only the portion of the power reported in Table 4 which is actually produced in the fuel is considered, i.e. approximately 93/94%; the remaining portion is used to calculate the temperature gain of the lead in the following way: a temperature increase is calculated which is then added to the nominal inlet temperature (400°C) so to preserve the heat balance of lead and the temperature difference between coolant and clad. All this is necessary because in ANTEO+ all the power is generated in the fuel. The nominal flow rate has been deduced by a new gagging scheme coherent with the new power distribution; for each FA the flow rate giving a coolant bulk temperature increase of 80°C has been calculated for both BoC and EoC. The average of the two configurations has been taken and plotted in order to easily identify the FAs with similar flow rates; from this, four cooling groups have been defined, which are characterized by the average of the flow rates of each FA composing the group. Since the power is more peaked in the core center, in the new gagging scheme the flow has been increased for the central FAs with respect to the LEADER version.

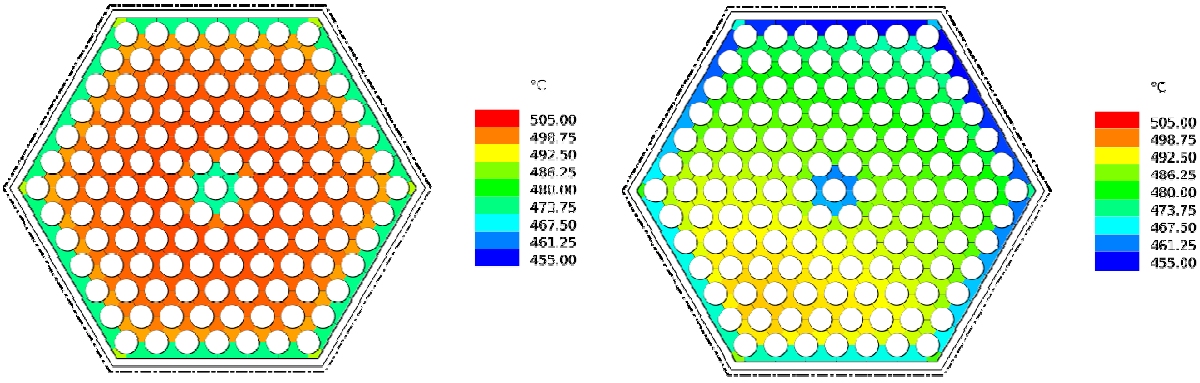

Figure 10 – BoC lead temperature distribution at core outlet in the hottest FAs of the INN (left) and OUT (right) core regions.

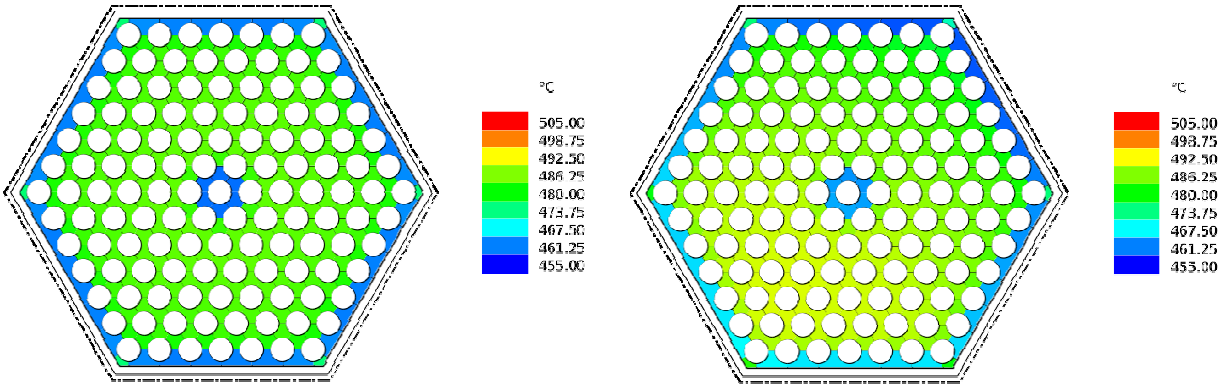

Figure 11 – EoC lead temperature distribution at core outlet in the hottest FAs of the INN (left) and OUT (right) core regions.

Results of the verification analysis are reported in Figures 10-11 and Table 5 where the effect of uncertainties coming from physical properties, geometry, power distributions, measurements and control systems dead bands are taken into account with a semi-statistical vertical approach in the evaluation of the maximum cladding temperature. In particular, the 3σ uncertainties for the bulk lead temperature gain is 20% while for the clad-bulk is around 38%.

Table 5 – Outlet lead and cladding temperatures.

State	BoC		EoC	
Region	INN	OUT	INN	OUT
Lead avg outlet	494	481	479	481
Lead max outlet	501	495	485	491
Cladding max	523	522	502	513
Cladding max + uncertainties	550	551	525	540

As can be seen, all the imposed temperature constraints are basically respected even when uncertainties are taken into account, thus proving the effectiveness of the proposed core configuration in steady state situations.

6. Conclusions

Closing the path delineated in the last two years of the Programmatic Agreement, the core of ALFRED as emerged from the LEADER project has been critically revised in a large spectrum of aspects in order to arrive to a core configuration mature enough to be taken as reference for the conceptual design stage. In this work the neutronic characterization of the new ALFRED core has been presented with the aim of flattening as much as possible the maximum clad temperature at pin level taking into account both CR movements during irradiation and uncertainties. DPA calculations for the critical components inside the vessel have also been reported, successfully complying with the design constraints.

In order to check the consistency of the adopted design methodology and to ensure that the temperature constraints are effectively met under steady state conditions, a detailed analysis at FA level has been performed. The thermal-hydraulic verification has revealed the robustness of the proposed configuration in nominal conditions where all the temperature-related constraints have been respected.

Concluding, the ALFRED core configuration here described is proposed as new reference for future analysis, remembering that further work will include the calculation of all the reactivity coefficients followed by a detailed safety analysis to test the degree of forgiveness to be reckoned to the plant design as a whole.

References

[1] U.S. Department Of Energy Nuclear Energy Research Advisory Committee and Generation IV International Forum. A Technology Roadmap for Generation IV Nuclear Energy Systems. Technical Report GIF(2002), http://www.gen-4.org/Technology/roadmap.htm.

[2] G. Grasso *et al*. A core design approach aimed at the sustainability and intrinsic Safety of the European Lead-cooled Fast Reactor. In Proceedings of *Fast Reactors and Related Fuel Cycles: Safe Technologies and Sustainable Scenarios* (*FR13*), Paris, France, March 4-7, 2013.

[3] G. Grasso *et al*. Demonstrating the effectiveness of the European LFR concept: the ALFRED core design. In Proceedings of *Fast Reactors and Related Fuel Cycles: Safe Technologies and Sustainable Scenarios* (*FR13*), Paris, France, March 4-7, 2013.

[4] E. Bubelis *et al*. LFR safety approach and main ELFR safety analysis results. In Proceedings of *Fast Reactors and Related Fuel Cycles: Safe Technologies and Sustainable Scenarios* (*FR13*), Paris, France, March 4-7, 2013.

[5] G. Grasso, F. Lodi et al. Ottimizzazione del progetto di nocciolo di ALFRED. Ricerca di Sistema Elettrico, Technical Report ADPFISS-LP2-050, 2014.

[6] F. Lodi, G. Grasso, D. Mattioli, M. Sumini. ANTEO+: a subchannel code for thermal-hydraulic analysis of liquid metal cooled systems. NED-D-15-00315 Under Review, Nuclear Engineering and Design, 2015.

Appendix - Simulation tools for the assessment of the stability and the dynamics of the new ALFRED configuration

In this section, the simulation tool devoted to the stability analysis is described along with the procedure adopted to perform the linear stability analysis. The stability analysis has been carried out both for the stand-alone core and the coupled primary loop configuration. Moreover, the impact of the coolant density reactivity coefficient on stability has been evaluated by considering both configurations. Such a study has been meant to provide the reactor designer with quantitative feedbacks concerning this key parameter from a safety-related perspective. Indeed, being the coefficient tightly dependent on the core arrangement, in terms of both geometrical and material buckling, it is expected that significant differences may occur between the demonstrator and the industrial scale LFR, with consequent impact on dynamics. Therefore, the system stability has been investigated against the lead density reactivity coefficient value in order to assess a theoretical threshold making the reactor unstable, so that the core designer can adopt suitable provisions to ensure the reactor operates under stable conditions in any situation beyond nominal. Finally, in order to evaluate the dynamic characteristics of the system as a function of the core lifetime, calculations have been carried out at BoC and EoC, so as to assess also the effects of the fuel burn-up.

A.1. Model development

An analytical zero-dimensional model accounting of all the main feedbacks following a reactivity change in the core has been implemented incorporating a point-wise kinetics description for neutronics coupled with a single-channel, average-temperature heat transfer treatment for thermal-hydraulics.

A.1.1. Neutronics

Point-wise kinetics with one neutron energy group and eight delayed neutron precursor groups has been employed for the core neutronics model, in which the total power is considered as generated only by fission events, while the contribution of decay heat being neglected.

In the present model scheme, a further simplified version has been adopted, in which all the precursor groups have been collapsed into a unique one, by means of an abundance-weighted average decay constant (Hetrick, 1971).

The main drawback of this model is the impossibility to describe a spatial dependence of the neutron population behavior, since the relationship between the latter and thermal power prevents from mapping the thermal power density within the core.

A.1.2. Thermal-hydraulics

A zero-dimensional approach has been adopted to treat also the system thermal-hydraulics. Some simplifying hypotheses have been assumed and a single-node heat transfer model has been implemented by accounting of three distinct temperature regions – corresponding to fuel, coolant and cladding –, enabling the reactivity feedback to include all the major contributions as well as the margin against technological limits to be monitored. In line with

the point model concept, the latter temperatures have been assumed to be functions separable in space and time.

Furthermore, a separate, multi-zone pin model accounting of the temperature distribution from the fuel centerline to the coolant bulk has been employed to calculate global heat transfer coefficients, by assuming physical properties and thermal resistances of fuel, gap and cladding to be constant with temperature and time, and neglecting thermal diffusion in the axial direction within the fuel pin.

As far as the dynamic variation of the fuel internal and external temperatures is concerned, the heat transfer process has been achieved by taking an energy balance over two fuel zones, where the fission power generated within the fuel is taken from the neutron kinetics equations and is treated as an input for the heat transfer dynamic model.

For the gradient of the cladding surface temperature, an energy balance has been applied.

Finally, for the energy balance equation within the coolant, the respective temperature at the end of the channel has been assumed as a state variable; being the coolant inlet temperature a fixed input, an energy balance has been written as well.

Calculations of material properties have been performed in correspondence with the average nominal steady-state temperatures and the parameters obtained have been kept constant for the stability analyses.

A.1.3. Reactivity

Consistently with the lumped parameter modeling employed, the reactivity feedback function has been expressed as a function of the average values of fuel and coolant temperatures. Moreover, externally introduced reactivity has been simulated by the coefficient associated with the insertion length of a representative control rod, which has been handled as a simple input parameter.

As far as the Doppler coefficient determination is concerned, an effective average fuel temperature that accounts for resonances broadening, has been calculated at each power level (ranging from 10 % to 100 % nominal) as indicated by Kozlowski and Downar (2007) as a function of the internal and external surface fuel temperatures. The magnitude of the actual reactivity variation from a generic fuel temperature distribution to another specific one around the steady-state value has been evaluated based on (Waltar et al., 2012), allowing to define the Doppler coefficient at each power level.

In this work, a linear relation for core expansions (axial and radial) and coolant density reactivity effects has been adopted, leading to an expression incorporating constant coefficients and where stationary average temperatures have been calculated in correspondence with each power level considered.

A.1.4. Primary loop

In order to evaluate the system stability when considering also the entire primary loop configuration, a simplified treatment has been adopted to describe the coolant flowing towards the Steam Generator (SG) after being heated in the core, being cooled while passing through the SG and coming back to the core through the cold leg and coolant pool.

In particular, the corresponding characteristic time delays have been introduced and the power exchange at the SG has been modeled by incorporating an equivalent exchange unit and taking its energy balance. More specifically, the SG has been modeled so that in nominal conditions the difference between core outlet and inlet coolant temperature is equal to the nominal value (80°C), whereas in ideal heat exchange conditions the cold leg temperature is kept constant and equal to the saturation temperature of the secondary loop, which depends only on SG pressure, regardless of the power produced in the core. In such a system, the coolant core inlet temperature is no longer an input variable, but a state variable determined by the power exchange conditions on the SG side. On the other hand, when "ideal heat exchange conditions" are considered, the SG is assumed to be able to remove any power produced in the core, thus keeping the lead temperature in the cold leg always close to the nominal value (i.e. 400°C).

A.2. Method

The analytical zero-dimensional model introduced above has been simplified and linearized so as to enable the use of the linear analysis theory to verify the reactor stability on the entire power range and in different conditions through calculation of the system eigenvalues.

According to the linear analysis theory, the dynamic behavior of a linear system depends on the eigenvalues of the state matrix. This principle is still applicable to a linearization of a non-linear system around a certain steady state condition (Lyapunov, 1966). Thus, such linearization has been performed on the set of equations associated to the phenomena and assumptions previously described, and it has been possible to express the model in terms of the following matrix system:

$$\begin{cases} \dot{x} = Ax + Bu \\ y = Cx + Du \end{cases}$$

where x is the vector of the state variables, u the input vector, y the output vector, A the state matrix, B and C the corresponding matrices, and D is an empty matrix since there is no feedthrough between input and output variables. This allows to focus on the matrix A and its eigenvalues, which represent the carriers of the dynamic response of the system; the latter, alternatively defined as poles or roots of the system, have been calculated through proper MATLAB® (The MathWorks Inc., 2015) scripts.

The position of the poles and their trajectories across the Gauss plane describe the dynamic behavior of the reactor: in order for the system to be stable, it is necessary that all poles remain in the left hand side of the plane in any working condition and following any perturbation of the nominal parameters, as discussed in the following case studies (Lyapunov, 1966).

CIRTEN

Consorzio **I**nteruniversitario per la **R**icerca **TE**cnologica **N**ucleare

POLITECNICO DI MILANO

DIPARTIMENTO DI ENERGIA, Sezione INGEGNERIA NUCLEARE-CeSNEF

Simulation tools for the assessment of the stability and the dynamics of the new ALFRED configuration

Antonio Cammi, Stefano Lorenzi

CERSE-POLIMI RL 1602/2015

Milano, Settembre 2015

Lavoro svolto in esecuzione dell'Attività LP2.A.1_C
AdP MSE-ENEA sulla Ricerca di Sistema Elettrico - Piano Annuale di Realizzazione 2014
Progetto B.3.1 "Sviluppo competenze scientifiche nel campo della sicurezza nucleare e collaborazione ai programmi internazionali per il nucleare di IV generazione"

(this page is intentionally left blank)

Index

INTRODUCTION 4
LIST OF SYMBOLS 6
LIST OF FIGURES 10
LIST OF TABLES 14
1. STABILITY ANALYSIS TOOL 16
1.1 MODEL DEVELOPMENT 16
1.2 METHOD 21
1.3 RESULTS 22
2. OBJECT-ORIENTED SIMULATOR 30
2.1. OBJECT-ORIENTED APPROACH 31
2.2. MODEL DEVELOPMENT 33
2.3 FREE DYNAMICS SIMULATIONS 46
2.4 STABILITY ANALYSIS VERIFICATION 54
REFERENCES 60
CONCLUSIONS 62
APPENDIX A: ALFRED REACTOR DESCRIPTION 64

(this page is intentionally left blank)

Introduction

The Lead-cooled Fast Reactor (LFR) is under development worldwide as a very promising fast neutron system to be operated in a closed fuel cycle. As recognized by the European Sustainable Nuclear Energy Technology Platform (SNETP), the LFR development requires as a fundamental intermediate step the realization of a demonstration plant intended to prove the viability of the technology as well as the overall system behavior. Advanced reactor concepts cooled by Heavy Liquid Metals Coolants (HLMCs) offer a great potential for plant simplifications and higher operating efficiencies compared to other coolants, introducing however additional safety concerns and design challenges.

This work is grafted in the research activity of the Nuclear Reactor Group of the Politecnico di Milano on LFRs In the framework of the "characterization of the new ALFRED core configuration", the POLIMI effort has been spent in order to provide the designers with important feedbacks on the stability and dynamics of the reactor system. To this purpose, the simulation tools should be expressly meant for this phase of the new characterization of ALFRED reactor design, in which all the system specifications are reconsidered and thus are subject to modifications. Accordingly, the report is aimed at presenting two very flexible, straightforward and fast-running (i.e., without significant computational burden and implementation-related effort) simulation tools.

The first simulation tool is directed to the stability analysis and consist of an analytical lumped-parameter model incorporating a point-wise kinetics description for neutronics coupled with a single-channel, average temperature heat transfer treatment for thermal-hydraulics. The simplicity of the modelling, implemented in MATLAB, relies upon the fact that the model has to be linearize in order to study the stability.

The second simulation tool is devoted to study the dynamics and verifying the outcomes of the stability analysis with a higher level of modelling accuracy. To this end, an object-oriented model is proposed to be both accurate and fast-running. The overall plant simulator, incorporating also the BoP, consists of the following essential parts: core, steam generator,

primary and secondary pumps, cold and hot legs, cold pool, turbine, and condenser. The model is developed with the Modelica language in the Dymola environment.

For the time being, the investigations are focused on the final configuration of the LEADER project, which can be considered the starting point of the new characterization. Nevertheless, in the further activities, the simulation tools developed in this report are foreseen to be adopted to study and finalize the new configuration.

List of symbols

Latin Symbols

A	single channel coolant flow area [m^2]
A_{CR}	coefficient for the calibration of CRs [pcm]
A_{SR}	coefficient for the calibration of SRs [pcm]
A_v	flow area [m^2]
B_{CR}	coefficient for the calibration of CRs [m^{-1}]
Bo	boiling number [-]
c	average specific heat capacity [J kg^{-1} K^{-1}]
C_{CR}	coefficient for the calibration of CRs [-]
c_i	density of the i^{th} precursor group [cm^{-3}]
C_f	Fanning friction coefficient [-]
Co	Convection number [-]
d	density [kg m^{-3}]
D_{CR}	coefficient for calibration of CRs [pcm]
f	friction factor [-]
F_{Fl}	fluid-surface parameter
Fr_{LO}	Froude number with all flow as liquid
g	gravitational acceleration [m s^{-2}]
h	specific enthalpy [J kg^{-1}]
h_{cl}	Cladding-coolant global heat transfer coefficient [W K^{-1}]
h_{CR}	height of control rods [m]
h_{LO}	single-phase heat transfer coefficient with all flow as liquid [W m^{-2} K^{-1}]
h_{SR}	height of safety rods [m]
h_{TP}	two phase heat transfer coefficient [W m^{-2} K^{-1}]
i_{LG}	latent heat of vaporization [J kg^{-1}]
k	thermal conductivity [W m^{-1} K^{-1}]
K	pressure coefficient [m^{-2} s^{-2}]
K_D	Doppler constant [pcm]

K_{eq}	Equivalent exchange unit [W K^{-1}]
k_v	turbine admission valve coefficient [m s]
k_f	Fuel thermal conductivity [W m^{-1} K^{-1}]
k_{fc}	Fuel-gap-cladding global heat transfer coefficient [W K^{-1}]
L_{SR}	total length of SRs [m]
M	Mass [kg]
n	neutron density [cm^{-3}]
N	number of axial nodes [-]
Nu	Nusselt number [-]
P	Reactor thermal power [MW]
p	pressure [Pa]
Pe	Peclet number [-]
q	neutron source [cm^{-3} s^{-1}]
q"	heat flux [W m^{-2}]
q"'	thermal power density [W m^{-3}]
r	radial coordinate [m]
R	radius [m]
t	time [s]
T	average temperature [K]
u	fluid velocity [m s^{-1}]
w	mass flow rate [kg s^{-1}]
x	axial coordinate [m]
x_c	critical ratio [-]
x_v	vapour quality [-]
x_{SR}	height of SRs at full power [m]
z	elevation [m]

Greek Symbols

α_{CR}	radial cladding expansion reactivity coefficient [pcm K^{-1}]
α_{CZ}	axial cladding expansion reactivity coefficient [pcm K^{-1}]

α_D	Doppler reactivity feedback coefficient [pcm K^{-1}]
α_{Dia}	diagrid expansion reactivity coefficient [pcm K^{-1}]
α_{FZ}	axial fuel expansion reactivity coefficient [pcm K^{-1}]
α_H	Control rod reactivity feedback coefficient [pcm m^{-1}]
α_L	coolant density reactivity coefficient [pcm K^{-1}]
α_{Pad}	pad effect reactivity coefficient [pcm K^{-1}]
α_R	Radial expansion reactivity feedback coefficient [pcm K^{-1}]
α_Z	Axial expansion reactivity feedback coefficient [pcm K^{-1}]
α_{WR}	radial wrapper expansion reactivity coefficient [pcm K^{-1}]
α_{WZ}	axial wrapper expansion reactivity coefficient [pcm K^{-1}]
β	DNP total fraction [pcm]
β_i	DNP fraction of the i^{th} precursor group [pcm]
Λ	neutron generation time [s]
λ_c	coefficient of discharge [-]
λ_i	decay constant of the i^{th} precursor [s^{-1}]
ρ	reactivity [pcm]
ρ_0	reactivity margin stored in the core [pcm]
τ_{HL}	Hot leg coolant circulation time constant [s]
τ_{SG}	Steam generator coolant circulation time constant [s]
τ_{CL}	Cold leg and pool coolant circulation time constant [s]
φ	heat flux entering the tube (lateral surface) [W m^{-2}]
ω	tube perimeter [m]

Superscripts

D	Doppler
eff	effective
1,3	fuel internal and external regions

Subscripts

0	steady-state
c	cladding

CBD	convective boiling dominant
down	downstream
ext	external
f	fuel
g	gap
i	inner
in	inlet
int	internal
l	lead coolant
L	liquid
NBD	nucleate boiling dominant
o	outer
out	outlet
sat	saturation
sg	steam generator
up	upstream
V	vapour

List of figures

Figure 1. Conceptual feedback scheme employed to describe the stand-alone core behavior. 23

Figure 2. Root locus detailed view for the stand-alone core as a function of power level at BoC (left) and EoC (right). 24

Figure 3. Root locus for the stand-alone core as a function of power level with $0 < \alpha_L < 12$ pcm K^{-1} at BoC. 25

Figure 4. Conceptual feedback scheme employed to describe the primary loop behavior. 25

Figure 5. Root locus for the primary system as a function of power level at BoC, nominal SG conditions (left) and ideal exchange conditions (right). 26

Figure 6. Root locus for the primary system as a function of power level with $0 < \alpha_L < 7$ pcm K^{-1} at BoC, nominal SG conditions. 27

Figure 7. Root locus for the primary system as a function of power level with $0 < \alpha_L < 7$ pcm K−1 at BoC, ideal perfect exchange conditions. 28

Figure 8. ALFRED object-oriented model. 33

Figure 9. ALFRED core object-oriented model. 34

Figure 10. Fuel pin radial scheme for heat transfer modelling. 36

Figure 11. Calibration curve of control rods and safety rods. 36

Figure 12. Fuel assembly geometry (lengths are expressed in mm). 39

Figure 13. Detailed view of ALFRED core: representation of coolant channels. 40

Figure 14. ALFRED SG object-oriented model. 42

Figure 15. ALFRED reactor secondary side. 45

Figure 16. Variables evolution after a feedwater mass flow rate reduction: (a) SG pressure variation; (b) lead SG outlet temperature variation; (c) average lead temperature variation; (d) net reactivity variation; (e) core thermal power variation; (f) average fuel temperature variation; (g) core outlet temperature variation; (h) steam temperature variation. 48

Figure 17. Variables evolution after a variation of the turbine admission valve coefficient: (a) SG pressure variation; (b) lead SG outlet temperature variation; (c) net reactivity variation; (d) core thermal power variation; (e) core outlet temperature; (f) steam temperature variation. 51

Figure 18. Variables evolution after a step reactivity variation: (a) net reactivity variation; (b) core thermal power variation; (c) core outlet temperature variation; (d) steam temperature variation; (e) SG pressure variation; (f) lead SG outlet temperature variation; (g) average fuel temperature variation; (h) average lead temperature variation. 53

Figure 19. Variables evolution after a step reactivity variation, stand alone core with α_L = 9 pcm/K: (a) core thermal power variation; (b) net reactivity variation; (c) average fuel temperature variation; (d) average lead temperature variation. 55

Figure 20. Variables evolution after a step reactivity variation, stand alone core with α_L = 13 pcm/K: (a) core thermal power variation; (b) net reactivity variation; (c) average fuel temperature variation; (d) average lead temperature variation. 55

Figure 21. Variables evolution after a step reactivity variation, stand alone core with α_L = 13 pcm/K at reduced power level: (a) core thermal power variation; (b) net reactivity variation; (c) average fuel temperature variation; (d) average lead temperature variation. 56

Figure 22. Variables evolution after a step reactivity variation, primary loop with α_L = 2 pcm/K: (a) core thermal power variation; (b) net reactivity variation; (c) average fuel temperature variation; (d) average lead temperature variation. 57

Figure 23. Variables evolution after a step reactivity variation, primary loop with α_L = 7 pcm/K: (a) core thermal power variation; (b) net reactivity variation; (c) average fuel temperature variation; (d) average lead temperature variation. 58

Figure 24. Variables evolution after a step reactivity variation, primary loop with α_L = 7 pcm/K at reduced power level: (a) core thermal power variation; (b) net reactivity variation; (c) average fuel temperature variation; (d) average lead temperature variation. 59

Figure 25. ALFRED nuclear power plant layout 64

Figure 26. ALFRED core configuration. 66

Figure 27. ALFRED bayonet tube SG configuration 67

(this page is intentionally left blank)

List of tables

Table 1. Main features and differences between causal and acausal approach.....32

Table 2. ALFRED core parameters.....65

Table 3. ALFRED SG major nominal parameters. 67

(this page is intentionally left blank)

1. Stability analysis tool

In this section, the simulation tool devoted to the stability analysis is described along with the procedure adopted to perform the linear stability analysis. The stability analysis has been carried out both for the stand-alone core and the coupled primary loop configuration. Moreover, the impact of the coolant density reactivity coefficient on stability has been evaluated by considering both configurations. Such a study has been meant to provide the reactor designer with quantitative feedbacks concerning this key parameter from a safety-related perspective. Indeed, being the coefficient tightly dependent on the core arrangement, in terms of both geometrical and material buckling, it is expected that significant differences may occur between the demonstrator and the industrial scale LFR, with consequent impact on dynamics. Therefore, the system stability has been investigated against the lead density reactivity coefficient value in order to assess a theoretical threshold making the reactor unstable, so that the core designer can adopt suitable provisions to ensure the reactor operates under stable conditions in any situation beyond nominal. Finally, in order to evaluate the dynamic characteristics of the system as a function of the core lifetime, calculations have been carried out at BoC and EoC, so as to assess also the effects of the fuel burn-up.

1.1 Model development

An analytical zero-dimensional model accounting of all the main feedbacks following a reactivity change in the core has been implemented incorporating a point-wise kinetics description for neutronics coupled with a single-channel, average-temperature heat transfer treatment for thermal-hydraulics.

1.1.1 Neutronics

Point-wise kinetics with one neutron energy group and eight delayed neutron precursor groups has been employed for the core neutronics model, in which the total power is considered as generated only by fission events, while the contribution of decay heat being neglected:

$$\frac{dn(t)}{dt} = \frac{\rho(t)-\beta}{\Lambda} n(t) + \sum_{i=1}^{8} \lambda_i c_i(t) \qquad (1)$$

$$\frac{dc_i(t)}{dt} = \frac{\beta_i}{\Lambda} n(t) - \lambda_i c_i(t) \quad (2)$$

Equations (1) and (2) represent nine Ordinary Differential Equations (ODEs): Eq. (1) is a nonlinear equation for neutron density and Eqs. (2) are linear equations for precursor densities.

In the present model scheme, a further simplified version has been adopted, in which all the precursor groups have been collapsed into a unique one, by means of an abundance-weighted average decay constant (Hetrick, 1971):

$$\frac{1}{\lambda} = \frac{1}{\beta}\sum_{i=1}^{8}\frac{\beta_i}{\lambda_i} \quad (3)$$

The main drawback of this model is the impossibility to describe a spatial dependence of the neutron population behavior, since the relationship between the latter and thermal power prevents from mapping the thermal power density within the core.

1.1.2 Thermal-hydraulics

A zero-dimensional approach has been adopted to treat also the system thermal-hydraulics. Some simplifying hypotheses have been assumed and a single-node heat transfer model has been implemented by accounting of three distinct temperature regions – corresponding to fuel, coolant and cladding –, enabling the reactivity feedback to include all the major contributions as well as the margin against technological limits to be monitored. In line with the point model concept, the latter temperatures have been assumed to be functions separable in space and time.

Furthermore, a separate, multi-zone pin model accounting of the temperature distribution from the fuel centerline to the coolant bulk has been employed to calculate global heat transfer coefficients, by assuming physical properties and thermal resistances of fuel, gap and cladding to be constant with temperature and time, and neglecting thermal diffusion in the axial direction within the fuel pin.

As far as the dynamic variation of the fuel internal and external temperatures is concerned, the heat transfer process has been achieved by taking an energy balance over two fuel zones:

$$M_{f,int} c_f \frac{dT_f^{int}(t)}{dt} = P_{int}(t) - k_f(T_f^{int}(t) - T_f^{ext}(t)) \quad (4)$$

$$M_{f,ext} c_f \frac{dT_f^{ext}(t)}{dt} = P_{ext}(t) + k_f(T_f^{int}(t) - T_f^{ext}(t)) - k_{fc}(T_f^{ext}(t) - T_c(t)) \quad (5)$$

where the fission power generated within the fuel is taken from the neutron kinetics equations according to Eq. (6), in which the subscript *0* indicates steady-state values, and is treated as an input for the heat transfer dynamic model:

$$\frac{n(t)}{n_0} = \frac{P(t)}{P_0} \tag{6}$$

For the gradient of the cladding surface temperature, the following energy balance has been applied:

$$M_c c_c \frac{dT_c(t)}{dt} = k_{fc}(T_f^{ext}(t) - T_c(t)) - h_{cl}\left(T_c(t) - T_{l,out}(t)\right) \tag{7}$$

Finally, for the energy balance equation within the coolant, the respective temperature at the end of the channel has been assumed as a state variable; being the coolant inlet temperature a fixed input, the energy balance has been written as:

$$M_l c_l \frac{dT_{l,out}(t)}{dt} = h_{cl}\left(T_c(t) - T_{l,out}(t)\right) - wc_l\left(T_{l,out}(t) - T_{l,in}(t)\right) \tag{8}$$

Calculations of material properties have been performed in correspondence with the average nominal steady-state temperatures and the parameters obtained have been kept constant for the stability analyses.

1.1.3 Reactivity

Consistently with the lumped parameter modeling employed, the reactivity feedback function has been expressed as a function of the average values of fuel and coolant temperatures. Moreover, externally introduced reactivity has been simulated by the coefficient α_H associated with the insertion length of a representative control rod, which has been handled as a simple input parameter.

As far as the Doppler coefficient determination is concerned, an effective average fuel temperature that accounts for resonances broadening, has been calculated at each power level (ranging from 10 % to 100 % nominal) as indicated by Kozlowski and Downar (2007).

$$T_f^{eff} = 0.3 \cdot T_f^{int} + 0.7 \cdot T_f^{ext} \tag{9}$$

(where T_f^{int} and T_f^{ext} indicate the internal and external surface fuel temperatures, respectively), and the magnitude of the actual reactivity variation from a generic fuel temperature distribution T_{f1} (with effective average T_{f1}^{eff}) to a fuel temperature distribution T_{f2} (with effective average T_{f2}^{eff}) around the steady-state value has been evaluated by:

$$\Delta\rho\,[T_{f1} \rightarrow T_{f2}] \approx 1.1 \cdot K_D \left(\ln \frac{T_{f2}^{\,eff}}{T_{f1}^{\,eff}}\right) \qquad (10)$$

based on (Waltar et al., 2012) where $\Delta\rho$ is expressed in [pcm].

Therefore, the Doppler coefficient has been defined at each power level as:

$$\alpha_D[\text{pcm K}^{-1}] = \frac{\Delta\rho[T_{f1} \rightarrow T_{f2}]}{T_{f2}^{\,eff} - T_{f1}^{\,eff}} \qquad (11)$$

In this work, a linear relation for core expansions (axial and radial) and coolant density reactivity effects has been adopted, leading to the following expression incorporating constant coefficients:

$$\rho(t) = \rho_0 + 1.1 \cdot K_D \left(\ln \frac{T_f^{\,eff}(t)}{T_{f0}^{\,eff}}\right) + \alpha_Z (T_f(t) - T_{f0}) + \alpha_R (T_l(t) - T_{l0}) +$$

$$+\alpha_L (T_l(t) - T_{l0}) + \alpha_H \left(h_{CR}(t) - h_{CR,0}\right) \qquad (12)$$

where stationary average temperatures (indicated by the subscript *0*) have been calculated in correspondence with each power level considered.

In Eq. (12) ρ_0 indicates the reactivity margin stored in the core; the second and the third terms in the right-hand side represent the feedbacks induced by fuel temperature changes (*i.e.*, Doppler effect and axial expansion, respectively), whereas the fourth and the fifth terms represent the feedbacks induced by coolant temperature variations (*i.e.*, lead density and radial expansion, respectively); the last term is the user-defined CRs reactivity.

1.1.4 Primary Loop

In order to evaluate the system stability when considering also the entire primary loop configuration, a simplified treatment has been adopted to describe the coolant flowing towards the SG after being heated in the core, being cooled while passing through the SG and coming back to the core through the cold leg and coolant pool.

In particular, the corresponding characteristic time delays have been introduced and the power exchange at the SG has been modeled by incorporating an equivalent exchange unit (subscript *eq*) and taking an energy balance as follows:

$$\frac{dT_{l,in\ SG}}{dt} = -\frac{1}{\tau_{HL}} T_{l,in\ SG} + \frac{1}{\tau_{HL}} T_l \quad (13)$$

$$\frac{dT_{l,out\ SG}}{dt} = \frac{\Gamma C_l - K_{eq}}{M_{eq} c_{eq}} T_{l,in\ SG} - \frac{\Gamma}{M_{eq}} T_{l,out\ SG} + \frac{K_{eq}}{M_{eq} c_{eq}} T_{sat} \quad (14)$$

More specifically, the SG has been modeled so that in nominal conditions the difference between core outlet and inlet coolant temperature is equal to the nominal value (80 °C), whereas in ideal heat exchange conditions the cold leg temperature is kept constant and equal to the saturation temperature of the secondary loop T_{sat} which depends only on SG pressure, regardless of the power produced in the core. In such a system, the coolant core inlet temperature is no longer an input variable, but a state variable determined by the power exchange conditions on the SG side:

$$\frac{dT_{l,in}}{dt} = -\frac{1}{\tau_{CL}} T_{l,in} + \frac{1}{\tau_{CL}} T_{l,out\ SG} \quad (15)$$

On the other hand, when "ideal heat exchange conditions" are considered, the SG is assumed to be able to remove any power produced in the core, thus keeping the lead temperature in the cold leg always close to the nominal value (*i.e.*, 400 °C).

1.2 Method

The analytical zero-dimensional model introduced above has been simplified and linearized so as to enable the use of the linear analysis theory to verify the reactor stability on the entire power range and in different conditions through calculation of the system eigenvalues.

According to the linear analysis theory, the dynamic behavior of a linear system depends on the eigenvalues of the state matrix. This principle is still applicable to a linearization of a non-linear system around a certain steady state condition (Lyapunov, 1966). Thus, such linearization has been performed on the set of equations presented in Section 3 and it has been possible to express the model in terms of the following matrix system:

$$\begin{cases} \dot{x} = Ax + Bu \\ y = Cx + Du \end{cases} \tag{16}$$

where *x* is the vector of the state variables, *u* the input vector, *y* the output vector, *A* the state matrix, *B* and *C* the corresponding matrices, and D is an empty matrix since there is no feedthrough between input and output variables. This allows to focus on the matrix *A* and its eigenvalues, which represent the carriers of the dynamic response of the system; the latter, alternatively defined as poles or roots of the system, have been calculated through proper MATLAB ® (The MathWorks Inc., 2015) scripts.

The position of the poles and their trajectories across the Gauss plane describe the dynamic behavior of the reactor: in order for the system to be stable, it is necessary that all poles remain in the left hand side of the plane in any working condition and following any perturbation of the nominal parameters, as discussed in the following case studies (Lyapunov, 1966).

1.3 Results

Six different conditions have been considered to draw the poles of the system. In the first place, a stand-alone core configuration has been studied, in this case the inlet temperature is considered as a fixed input. In this condition, three major cases have been analyzed:

a) power level ranging between zero power and full nominal power at BoC;

b) power level ranging between zero power and full nominal power at EoC;

c) parametric variation of the lead density reactivity coefficient on the entire power range at BoC.

In the second place, the simplified primary system configuration has been taken into account, and the effects of closing the loop on stability have been assessed. Similarly to the stand-alone core study, three cases have been considered:

a) power level ranging between zero power and full nominal power at BoC with SG at nominal conditions;

b) power level ranging between zero power and full nominal power at BoC with SG at ideal heat exchange conditions;

c) parametric variation of the lead density reactivity coefficient on the entire power range at BoC with SG at nominal conditions.

1.3.1 Stand-alone core analysis

A stand-alone core analysis has been carried out aimed at verifying the core system stability in nominal conditions at different power levels at BoC. In particular, the neutronics block has been treated as the open loop, whereas the thermal-hydraulics with its reactivity coefficients constitutes the feedback loop, as depicted in Figure 1.

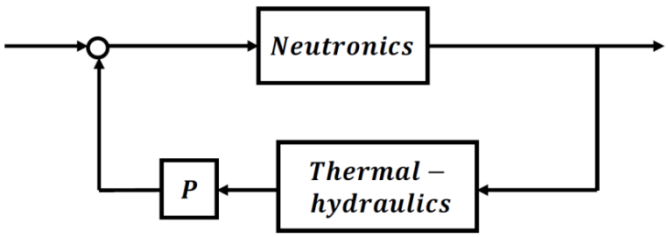

Figure 1. Conceptual feedback scheme employed to describe the stand-alone core behavior.

A thirteenth order system has been obtained by implementing Eqs. from (1)–(8); after simplification and linearization, a four roots system has been found: actually neutron precursors groups have been collapsed into a single one whose decay constant is provided by Eq.(3), and the cladding contribution has been simply neglected.

All the system roots lay on the left hand side of the Gauss plane, confirming that the core is stable on the entire power range (Poles at -4700 rad s^{-1} and -2.5 rad s^{-1} are not shown and discussed in this analysis since they do not change their position significantly with varying power and lead coefficient, resulting in an almost constant contribution to the system behaviour.).

More in detail, the neutronics-related pole is located in the origin when the reactor is at zero power conditions, and moves to the left as the power rises, due to the increasing effect of the temperature-induced negative reactivity feedbacks. At a certain power level the dominant poles become complex conjugated, as shown in Figure 2, indicating that power fluctuations occur. In particular, the imaginary part of the poles increases along with the rising power level, meaning that the frequency of the oscillations increases too. Despite the rise of the imaginary part of the poles, the magnitude of the real negative part grants the damping of such oscillations. This phenomenon ensues from the fact that in the linearized model the gain of the thermal feedback is proportional to the power level; thus, for equal variations of reactivity, the oscillation frequency grows as the power increases.

An analogous behavior is found at EoC, whose root locus is shown on the right side of Figure 2: the core exhibits the same stability characteristics as at BoC, coherently with the very slight differences between the respective reactivity coefficients and kinetic parameters. As a consequence of such minor discrepancies, it can be concluded that the influence of the fuel burn-up is definitely negligible as far as the system stability is concerned.

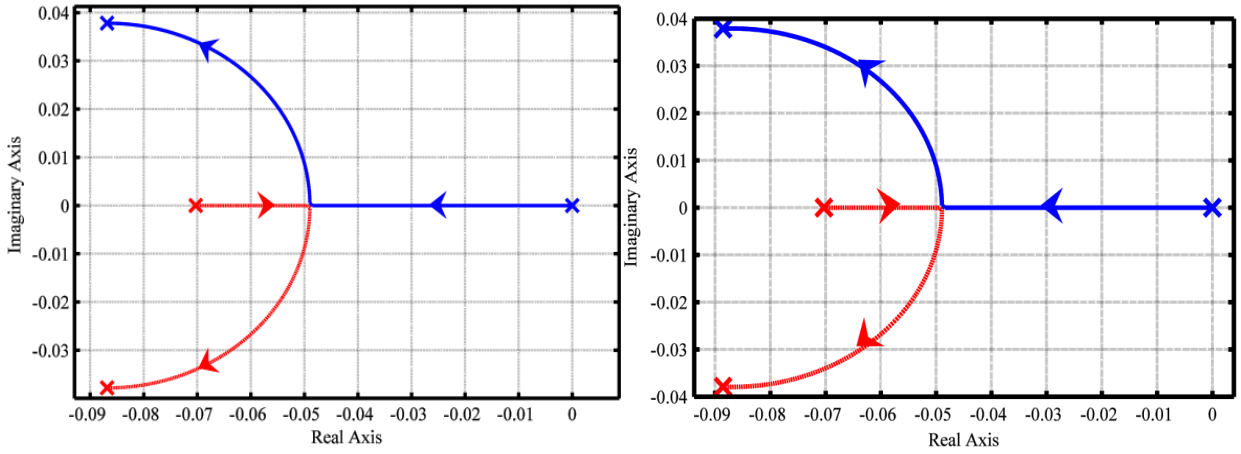

Figure 2. Root locus detailed view for the stand-alone core as a function of power level at BoC (left) and EoC (right).

The core system stability has been investigated also when making the coolant density reactivity coefficient parametrically vary from its positive nominal value to large positive figures, so as to determine a critical threshold rendering the system unstable.

As shown in Figure 3, the blue track represents the poles trajectory as a function of power level (from 0 to 300 MWth) with α_L kept constant at its nominal value. The red lines represent the poles trajectories evaluated at discrete power levels (from 30 MW_{th} to nominal power, with 10% steps) as a function of α_L varying from 0 to 12 pcm K^{-1}. In this latter case, for increasing values of the lead density coefficient, the roots move to the right, becoming first real and then also positive at a certain critical value around 12 pcm K^{-1}. Such a trend is not always the same since the critical value depends on the power level considered: actually, the system at nominal power becomes unstable for the lowest lead density coefficient (as described in Figure 3, black track). This trend is mainly due to the amplified feedback effects at higher power. In fact, if the action of a feedback is destabilizing (i.e., the corresponding reactivity coefficient is positive), its impact is first noticed at high power, where its magnitude is larger because more amplified. In addition, the (negative, that is stabilizing) Doppler effect is stronger at low power levels, and decreases along with the power level increase. Therefore, at low power levels there is a stronger counteraction by the Doppler effect, which counterbalances the lead density coefficient positive action. In other words, the core behavior is more sensitive to this design parameter variation at nominal power, and thus it may be concluded that, at low power levels, the system is more

robust to uncertainties affecting its value. In any case, it has been seen that the system becomes unstable only for extremely high values of α_L, a clearly non-realistic condition.

Therefore, it can be stated that the system is inherently stable, and consequently safe, both at low power levels and in the case of positive coolant density reactivity coefficients.

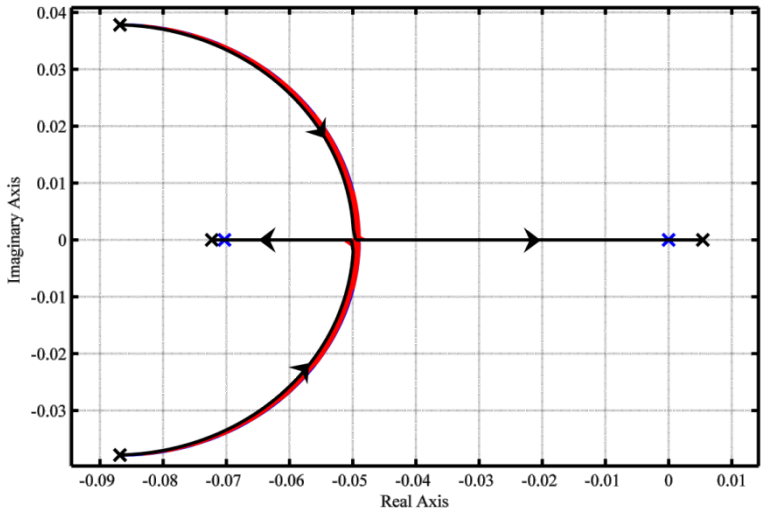

Figure 3. Root locus for the stand-alone core as a function of power level with $0 < \alpha_L < 12$ pcm K^{-1} at BoC.

1.3.2 Primary loop analysis

A stability analysis has been carried out also in a primary loop configuration in order to consider a more realistic situation in which the SG feedback action on the core dynamics is taken into account (Figure 4).

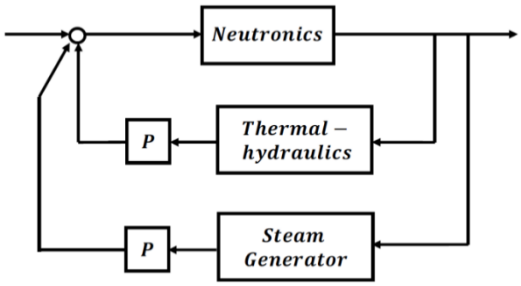

Figure 4. Conceptual feedback scheme employed to describe the primary loop behavior.

Eqs. (13)–(15) have been added to the previous set of equations to represent the influence of the SG and the closure of the primary loop, obtaining a total of sixteen equations. Also in this case,

model simplification and linearization have reduced the dimension of the equation set: finally, a seven roots system has been considered.

As Figure 5 illustrates, the system is still stable in nominal conditions at each power level, but compared to the previous case, additional complex conjugate poles appear in the plots: a new dynamics has been found on the right of the trajectories representing the stand-alone core; the new tracks are closer to the origin and complex conjugate for low power levels, suggesting that the dynamics they describe is slower and with damped oscillations In this case only one pole remains close to the origin also at high power levels, whereas in the stand-alone core analysis both the roots move to the left. As mentioned previously, when coupling the core with the SG the coolant core inlet temperature is no longer a fixed input, becoming instead a state variable depending on the power exchange conditions at the interface with the secondary side. This induces a feedback on the core behavior, whose neutronics is influenced by the reactivity effects led by temperature changes.

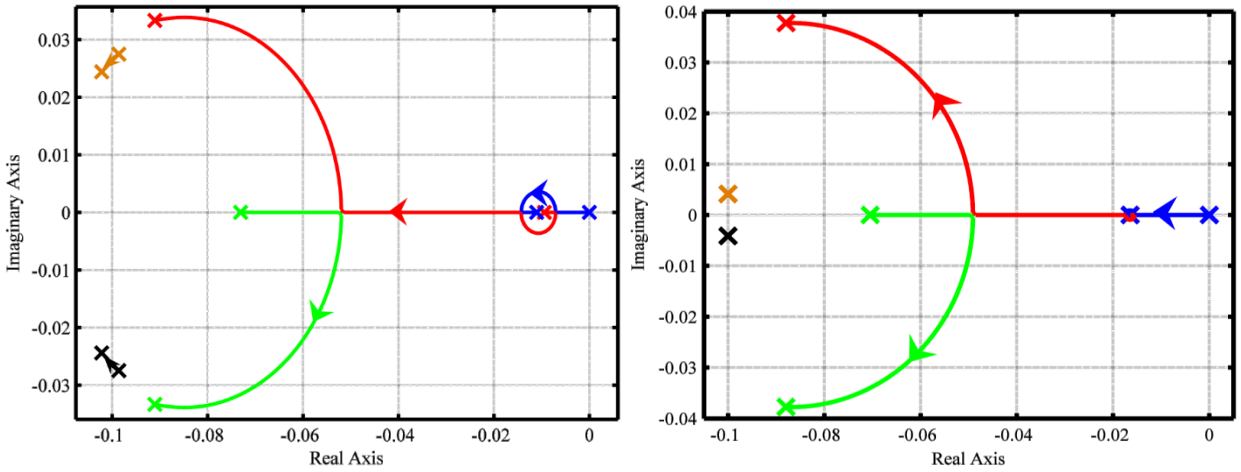

Figure 5. Root locus for the primary system as a function of power level at BoC, nominal SG conditions (left) and ideal exchange conditions (right).

When the SG is set at nominal conditions, any power variation on the core side causes the core inlet temperature to change affecting the system reactivity (primarily due to the coolant temperature variation, with a consequent additional lead density and radial expansion feedback), differently than in the stand-alone core case, in which the inlet temperature is a fixed input. Such phenomena explain the system new oscillatory behavior at low power shown in Figure 5.

In addition, the situation of ideal heat exchange conditions on the SG side have been considered (Figure 5, right graph): it clearly appears how, for increasing exchange capabilities, the circle moves to the left and reduces its dimensions, meaning that oscillations progressively damp as the stand-alone core case is asymptotically approached (i.e., inlet temperature independent of the SG heat exchange capabilities). In both the above mentioned situations, the primary loop pole trajectories have been examined again as a function of the lead density coefficient variation (Figure 6).

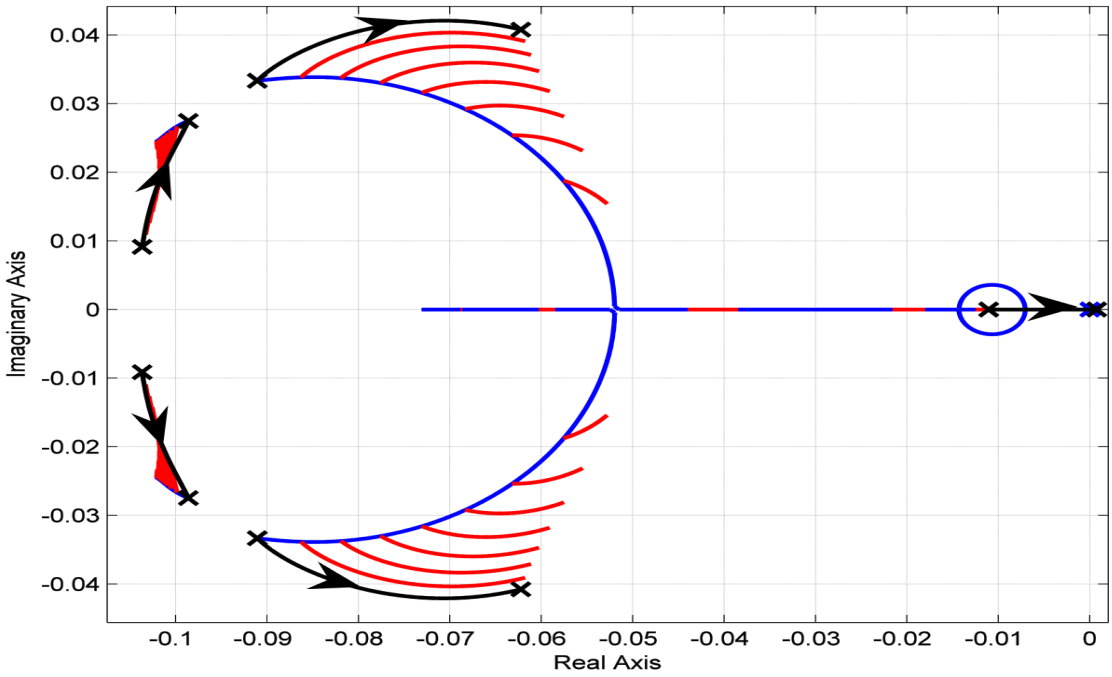

Figure 6. Root locus for the primary system as a function of power level with 0 < α_L < 7 pcm K^{-1} at BoC, nominal SG conditions.

As in the previous graphs, the blue track constitutes the roots trajectories when the power varies and α_L is equal to its nominal value, whereas red tracks represent the poles motion induced by variations of α_L from 0 to 7 pcm K^{-1} at each power level (the nominal power is depicted with black track).

By comparing Figure 6 with Figure 3,it can be inferred that the primary loop system behaves qualitatively as the stand-alone core one, but the instability threshold is reached earlier in the former case: for increasing values of the lead density coefficient the poles move to the right and

become real positive when α_L is between 6 and 7 pcm K^{-1}, evidencing a kind of "destabilizing" action by the SG.

In confirmation of this, the system stability has been analyzed by connecting a progressively more performing SG to the core, and it appears very clearly that the closer the heat exchange conditions are to the ideal ones, the higher is the margin of stability of the reactor system, since the core is less and less influenced by the secondary side dynamics. Indeed, when considering an ideal SG (Figure 7), the poles never reach a positive real part for the considered range of α_L, implying that greater values of the reactivity coefficient are needed for the system to become unstable, likewise in the only core case (Figure 3).

Anyway, even when considering the closed system configuration with nominal SG conditions, the reactor becomes unstable only for very high values of α_L, which are still non-realistic. Therefore, it can be definitely concluded that the overall system is indeed inherently stable, and consequently safe.

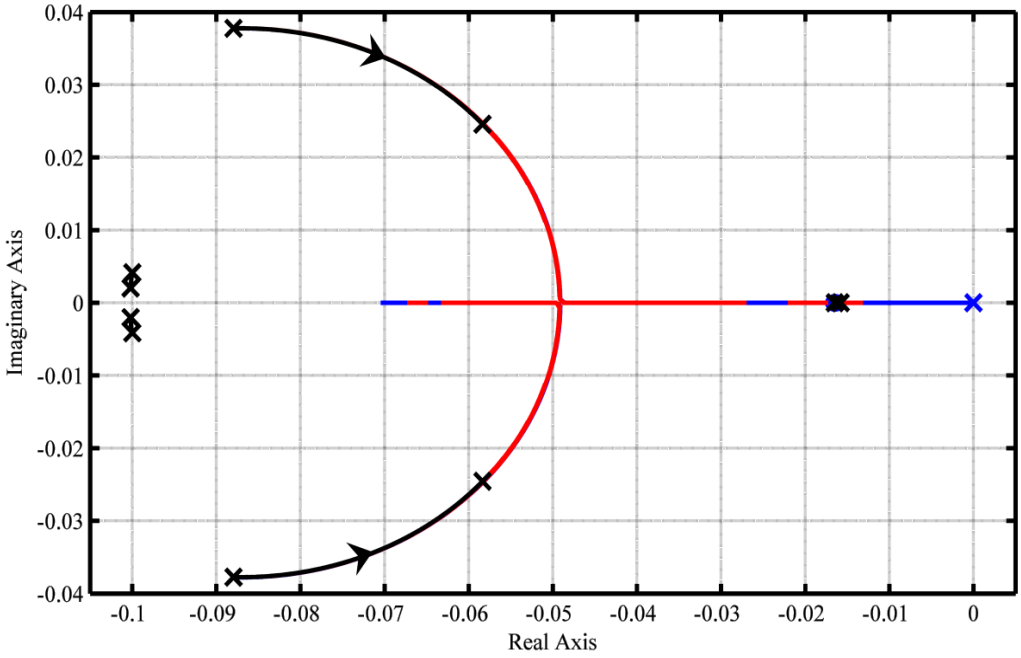

Figure 7. Root locus for the primary system as a function of power level with 0 < α_L < 7 pcm K−1 at BoC, ideal perfect exchange conditions.

(this page is intentionally left blank)

2. Object-oriented simulator

In order to properly characterize the ALFRED governing dynamics and to verify the stability outcomes of the lumped-parameter model, it has been necessary to develop an accurate simulation tool. Therefore, a simulator exploiting the object-oriented modelling has been developed. The overall plant model has been written in Modelica language and implemented in Dymola environment by assembling both component models already available in a specific thermal-hydraulic library, and specific nuclear component models suitably modified according to the ALFRED specification to provide the required capabilities for the analysis.

The primary circuit model has been built by connecting the above-mentioned components, taking into account suitable time delays, and incorporating the cold pool, which has revealed to be fundamental to allow for the system characteristic time constants. The plant simulator has been finalized by connecting standard turbine, condenser and other components of the Balance of Plant. This approach has been specifically addressed to transient analyses, since its more detailed geometry characterization ensures more accurate simulation outcomes. Different design-basis transient scenarios have been simulated to characterize the system free dynamics. In addition, the results of the previous stability analysis have been confirmed by proper simulations.

2.1. Object-oriented approach

The most important features (Cammi et al., 2005; Cammi and Luzzi, 2008) required to the modelling tool are the following: (i) modularity, in order to enhance the reusability of pre-existing and also validated components; (ii) openness, since the equations implemented have to be clearly readable; (iii) efficiency, meaning that the simulation code should be fast running; and (iv) integrability with the control system model.

A viable path to achieve the above-mentioned goals is constituted by the adoption of the Modelica language (Modelica, 2011). Introduced in 1997, Modelica is "a language for modelling and simulation of complex cyber-physical systems" (Fritzson, 2004). In particular, it is an object-oriented modelling approach specifically designed for the study of engineering system dynamics. In this perspective, Modelica facilitates the system description in terms of physical and engineering principles (i.e., mass, energy and momentum balance equations). Modelica is employed for the modelling of general physical phenomena described by sets of differential algebraic and discrete equations, supporting a declarative language. This feature allows acausal modelling, i.e., the direct use of equations without imposing the classic input/output declaration, granting a more flexible and efficient data flow (Fritzson, 2011). Finally, Modelica is open-source and it has already been successfully adopted in different fields, such as automotive, robotics, thermo-hydraulic and mechatronic systems, but also in nuclear simulation field (Cammi et al., 2005; Souyri et al., 2006).

One of the main advantages of employing the Modelica language is the possibility of adopting acausal modelling approach. The system dynamics is described in terms of conservation laws that, combined with the constitutive equations of the components, determine the overall set of equations to be solved. Thanks to the acausal modelling, the equations of each component model can be written independently from the definitions of input/output variables. Thus, the causality of equation-based models is unspecified and becomes fixed only when the corresponding equation systems have to be solved (Fritzson, 2004). In this way, models are much easier to write and reuse, while the burden of determining the actual sequence of computations required for the simulation is entirely left to the compiler. In the common practice, most of the present simulators

are based on causal modelling, e.g., MATLAB® and SIMULINK® (The MathWorks, 2015), whose main features are reported in Table 1.

Table 1. Main features and differences between causal and acausal approach.

Causal approach	Acausal approach
System input and output variables have to be established at the beginning	It is not necessary to establish *a priori* input and output variables
Equations have to be rewritten for each specific application in state space representation	Causality remains unspecified as long as equations have to be solved
Low flexibility in changing the model configuration	More realistic description of components and modularity
Low reusability of previous work. Problem formulation in a series of operations must be performed by the user, according to the particular applicative context	Possibility of easily reusing previously developed models. Components models are defined independent of their potential connections
Block diagram representation (physics-oriented)	Plant representation (component-oriented)
Integration algorithm for ordinary differential equations (lower computational cost)	Integration algorithm for differential algebraic equations (higher computational cost)
Low order modelling, easy to linearize (stability analyses)	Potentially high number of equations involved

In addition, the multi-physics approach of the Modelica language must be mentioned. General in scope, it provides modelling primitives such as generic algebraic, differential and difference equations, and it is not tied to any specific physical or engineering domain (i.e., mechanics, electrical engineering, or thermodynamics). Thus, it is quite straightforward to describe multi-disciplinary systems, e.g. the reactor core, where several physics (e.g., neutronics, heat exchange and fluid dynamics) interact with each other. Furthermore, a more realistic plant representation is made possible by the component-based description. As simulation environment, Dymola (Dynamic Modelling Laboratory) (Elmqvist et al., 1993) has been adopted, as dedicated libraries of validated models for power plant components are available.

As to the efficiency of the simulation code, Modelica compilers incorporate sophisticated symbolic manipulation algorithms, which allow to obtain index-1 systems of differential-algebraic equations from higher-index ones, to symbolically solve both linear and nonlinear model equations (Fritzson, 2004). The resulting code is then linked to state-of-the-art numerical integration codes such as DASSL (Brenan et al., 1989).

2.2. Model development

A non-linear one-dimensional model of the ALFRED reactor has been developed by adopting the object-oriented approach based on the Modelica language. The overall system model has been built by connecting the different components (objects) through rigorously defined interfaces (connectors) corresponding to specific physical interactions occurring with the external environment or other objects. The overall plant simulator, incorporating also the BoP, consists of the following essential parts: core, steam generator, primary and secondary pumps, cold and hot legs, cold pool, turbine, and condenser (Figure 8).

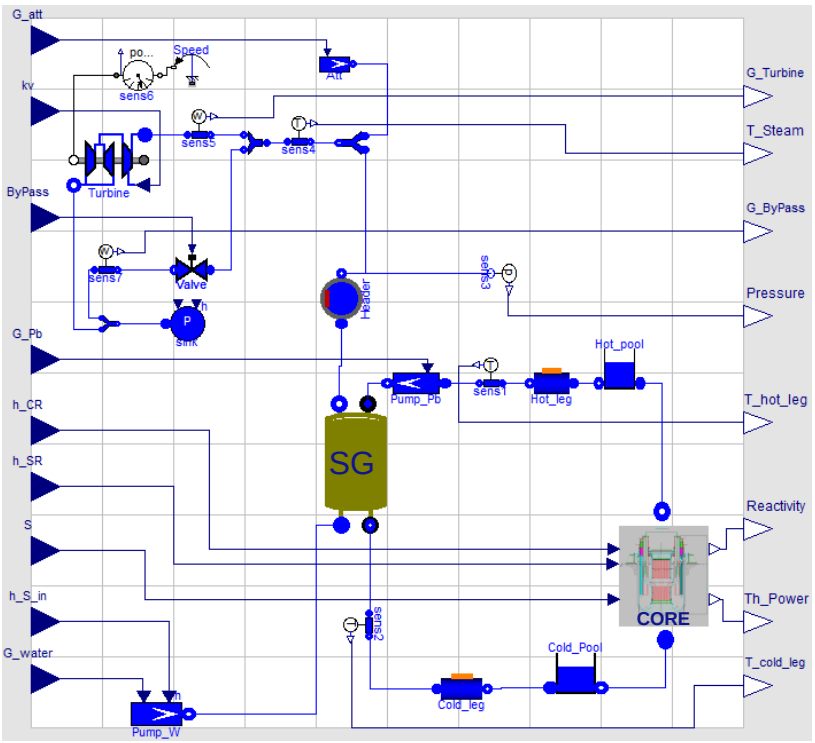

Component	Description
Core	Reactor core
Cold_pool	Pool collecting the lead coming from the SG outlet
Cold_leg	Collector between the SG outlet and the core inlet
Hot_pool	Pool collecting the lead coming from the core outlet
Hot_leg	Collector between the core outlet and the SG inlet
sens	Temperature and pressure sensor placed in the plant
Pump_Pb	Lead axial pump
SG	Steam generator
Header	Volume collecting the produced steam
Pump_W	Water pump
Turbine	Steam turbine unit
Sink	Condenser
Att	Attemperator that allows to regulate the steam temperature

Figure 8. ALFRED object-oriented model.

The primary and secondary systems have been modelled and implemented in Modelica by assembling conventional component models already available in a specific thermal-hydraulic library, named Thermopower (Casella et al., 2006), and specifically developed nuclear component models, taken from the NuKomp library (Cammi et al., 2005), modified in order to provide the required capabilities for the analysis. The resulting overall plant simulator,

incorporating also the BoP, consists of the following essential parts: core, steam generator, primary and secondary pumps, cold and hot legs, cold pool, turbine, and condenser.

2.2.1. Core

As far as the ALFRED core is concerned (Figure 9), point reactor kinetics and one-dimensional heat transfer models have been implemented, coherently with the plant specifications, by incorporating suitable geometry, material properties and correlations, neutronic feedback coefficients and kinetic parameters (see Appendix A).

The component-based core model is constituted by four sub-systems, each one dedicated to a particular physics. The component *Kinetics* employs a point reactor kinetics model with one neutron energy group and eight delayed precursor groups. Therefore, the neutron density evolution is described by the following equation:

$$\frac{dn}{dt} = \frac{\rho - \beta}{\Lambda} n + \sum_{i=1}^{8} \lambda_i c_i + q \qquad (16)$$

the corresponding concentration of precursors being expressed as

$$\frac{dc_i}{dt} = \frac{\beta_i}{\Lambda} n - \lambda_i c_i \qquad i = 1 \div 8 \qquad (17)$$

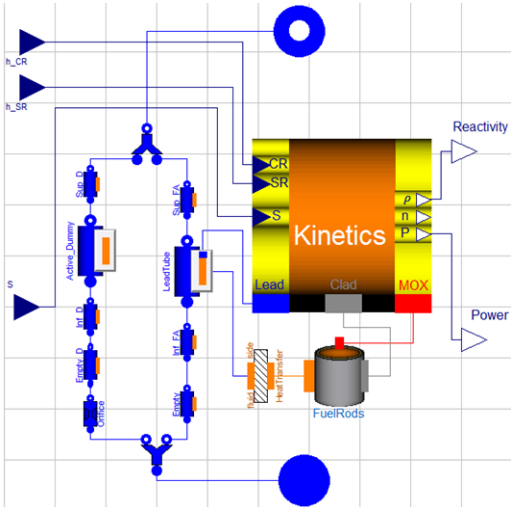

Figure 9. ALFRED core object-oriented model.

In the present model, two different definitions have been implemented to describe the effective fuel temperatures, and namely: $T_f{}^D$, which expresses the effective temperature to allow for the

Doppler effect, and $T_f^{\,eff}$, which represents the average temperature that allows to evaluate quantitatively the reactivity feedback due to the pellet deformation caused by thermal stresses. Therefore, as far as the Doppler reactivity contribution is concerned, an effective fuel temperature allowing for resonances broadening (Kozlowski and Downar, 2007) has been considered:

$$T_f^{\,D} = 0.3 \cdot T_f^{\,1} + 0.7 \cdot T_f^{\,3} \tag{18}$$

In Eq. (18), $T_f^{\,1}$ and $T_f^{\,3}$ represent the average temperatures in the central region and in the external one of the fuel pin, respectively (see Figure 10). In Eq. (19), the weights provide an estimate of the volume-weighted average behaviour, and have been used to reproduce the parabolic trend of the temperature field within the fuel pellets:

$$T_f^{\,eff} = (1/2) \cdot T_f^{\,1} + (1/2) \cdot T_f^{\,3} \tag{19}$$

The reactivity variation from a generic fuel temperature distribution T_{f1} (with effective average $T_{f1}^{\,D}$) to a fuel temperature distribution T_{f2} (with effective average $T_{f2}^{\,D}$), due to the Doppler effect, has been evaluated as follows (Waltar et al., 2012):

$$\Delta\rho\left[T_{f1} \rightarrow T_{f2}\right] \approx 1.1 \cdot K_D \left(\ln \frac{T_{f2}^{\,D}}{T_{f1}^{\,D}} \right) \tag{20}$$

Reactivity effects due to the coolant density variations, as well as to the axial and radial expansions, have been taken into account by adopting linear equations with constant coefficients. In particular, axial and radial cladding expansions have been related to the average cladding thermal conditions, while axial and radial wrapper expansions have been considered governed by the lead temperature. On the other hand, the grid expansion effect concerns the increase of the core radius due to the incoming coolant temperature enhancement. Therefore, the coolant volume inside core increases as well as the core volume and, in turn, the leakages. These combined effects determine an overall negative contribution. The pad effect is determined by the radial expansion difference between the bottom of the subassemblies at the incoming coolant temperature and their top at the outlet coolant temperature. However, this reactivity contribution is quite reduced (Grasso et al., 2014).

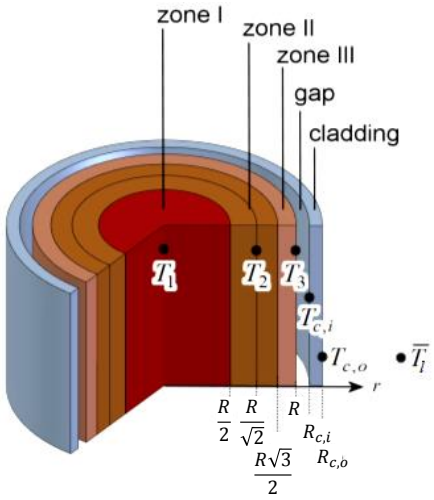

Figure 10. Fuel pin radial scheme for heat transfer modelling.

As far as the CRs are concerned, a reactivity differential curve has been adopted based on the reactivity worth of the 12 rods at different insertion lengths (Figure 11).

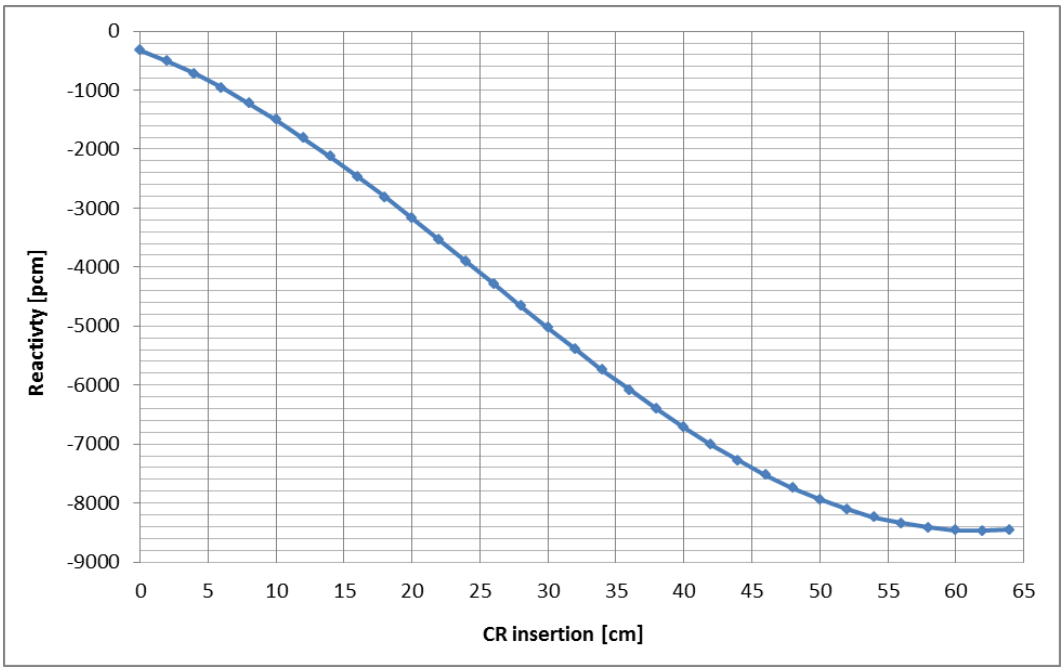

Figure 11. Calibration curve of control rods and safety rods.

On the other hand, worth characterization of SRs does not require such an accuracy, because these rods are extracted during start-up phase and then they are kept out of the core while the

reactor is operating at full power conditions. Consequently, a linear dependence of the reactivity as function of axial position is sufficient to describe the SR reactivity contribution.

The overall system reactivity is given by the sum of the various contributes, as follows:

$$\rho(t) = \rho_0 + \alpha_L \cdot \left(T_l - T_{l,0}\right) + 1.1 \cdot K_D \left(\ln \frac{T_{f2}^{\ D}}{T_{f1}^{\ D}} \right) + \alpha_{CZ} \cdot \left(T_C - T_{C,0}\right) + \alpha_{WZ} \cdot \left(T_l - T_{l,0}\right) +$$

$$+ \alpha_{CR} \cdot \left(T_C - T_{C,0}\right) + \alpha_{WR} \cdot \left(T_l - T_{l,0}\right) + \alpha_{FZ} \cdot \left(T_C - T_{C,0}\right) + \alpha_{Dia} \cdot \left(T_{l,in} - T_{l,in,0}\right) + \quad (21)$$

$$+ \alpha_{Pad} \cdot \left(T_{l,out} - T_{l,out,0}\right) + A_{CR} \cdot \sin\left(B_{CR} \cdot h_{CR} + C_{CR}\right) + D_{CR} + A_{SR} \cdot \frac{\left(h_{SR} - x_{SR}\right)}{L_{SR}}$$

The terms in Eq. (21) represent the effect due to lead density, Doppler effect, axial cladding expansion, axial wrapper expansion, radial cladding expansion, radial wrapper expansion, axial fuel expansion, diagrid expansion, pad effect, control rod contribution, safety rod contribution, and the initial reactivity margin, respectively.

The component *FuelRods* describes the thermal behaviour of the fuel pins, by adopting five radial regions within the element (i.e., cladding, gaseous gap and three concentric zones of equal volume within the pellet). The time-dependent Fourier equation is applied considering only the radial heat transfer, thus disregarding both the axial and the circumferential thermal diffusion. Fourier equation has been discretized radially in five zones and longitudinally in a user-defined number (*N*) of nodes.

$$d_f c_f \frac{\partial T_f}{\partial t} = \frac{1}{r} \frac{\partial}{\partial r} \left(r k_f \frac{\partial T_f}{\partial r} \right) + q''' \quad (22)$$

$$\frac{\partial}{\partial r} \left(r k_g \frac{\partial T_g}{\partial r} \right) = 0 \quad (23)$$

$$d_c c_c \frac{\partial T_c}{\partial t} = \frac{1}{r} \frac{\partial}{\partial r} \left(r k_c \frac{\partial T_c}{\partial r} \right) \quad (24)$$

The component *LeadTube* models the coolant flowing through the core channels represented as cylindrical conduits. It simulates a one-dimensional single-phase fluid flow with heat transfer

from the fuel pin boundary and with temperature-dependent physical properties (OECD-NEA, 2007). This approach is based on distributed-parameter mass, momentum and energy conservation equations discretized by employing a finite volume method.

$$A\frac{\partial d}{\partial t}+\frac{\partial w}{\partial x}=0 \tag{25}$$

$$\frac{\partial w}{\partial t}+A\frac{\partial p}{\partial x}+dgA\frac{\partial z}{\partial x}+\frac{C_f\omega}{2dA^2}w|w|=0 \tag{26}$$

$$dA\frac{\partial h}{\partial t}+dAu\frac{\partial h}{\partial x}-A\frac{\partial p}{\partial t}=\omega\varphi \tag{27}$$

Equations (25) and (26) describe the pressure and mass flow rate dynamics, while Eq. (27) describes the slower dynamics of heat transport with the fluid velocity.

The component *HeatTransfer* allows to evaluate the heat flux exchanged between two one-dimensional interacting objects (e.g., the fluid flow and metal wall) as a function of the corresponding surface temperatures. Since the fuel pins are arranged on a triangular lattice, the Ibragimov-Subbotin-Ushakov correlation (Cheng and Tak, 2006) has been adopted to properly estimate the convective heat transfer coefficient. Moreover, among the possible correlations, it is the most conservative one since gives the lowest value of the Nusselt number.

$$Nu=4.5+0.014\cdot Pe^{0.8} \tag{28}$$

In the ALFRED core, the presence of a *bypass mass flow rate* has been foreseen since it has a fundamental role in certain plant operational modes, such as the start-up phase. In the proposed configuration, the main part of the coolant passes through the fuel elements, while a reduced fraction passes through the interstices between the wrappers, and through the dummy elements and the cases of the CRs and the SRs. Indeed, the power is deposited not only in the fuel, but also in the other materials, mainly due to the γ emission. For these reasons, the lead mass flow rate devoted to the bypass has been fixed at the 3% of the one that circulates in the primary circuit. In a preliminary description, in order to represent the evolution of the temperature fields of the main components of the core, the presence of the bypass mass flow rate can be neglected. This approach can be suitable if the system is studied only in nominal operating conditions.

Nevertheless, in accidental scenarios or in operating conditions in which the lead mass flow rate is not kept constant at the nominal value (e.g., during the reactor start-up), a more accurate characterization of the pressure field is essential. In particular, in the core thermal-hydraulics description, two types of channels, which represent the fuel elements and the dummy elements, have been allowed for.

In the modelling of the channels, in order to reproduce the actual layout of the assemblies (Figure 12), different types of components (Figure 13) have been employed. Furthermore, a component that allows to impose additional pressure losses has been added to the dummy elements description. Since the channels are subjected to the same inlet and the outlet pressure field, hydraulic resistance at the entrance of dummy elements has been suitably tuned so as to achieve the desired pressure field.

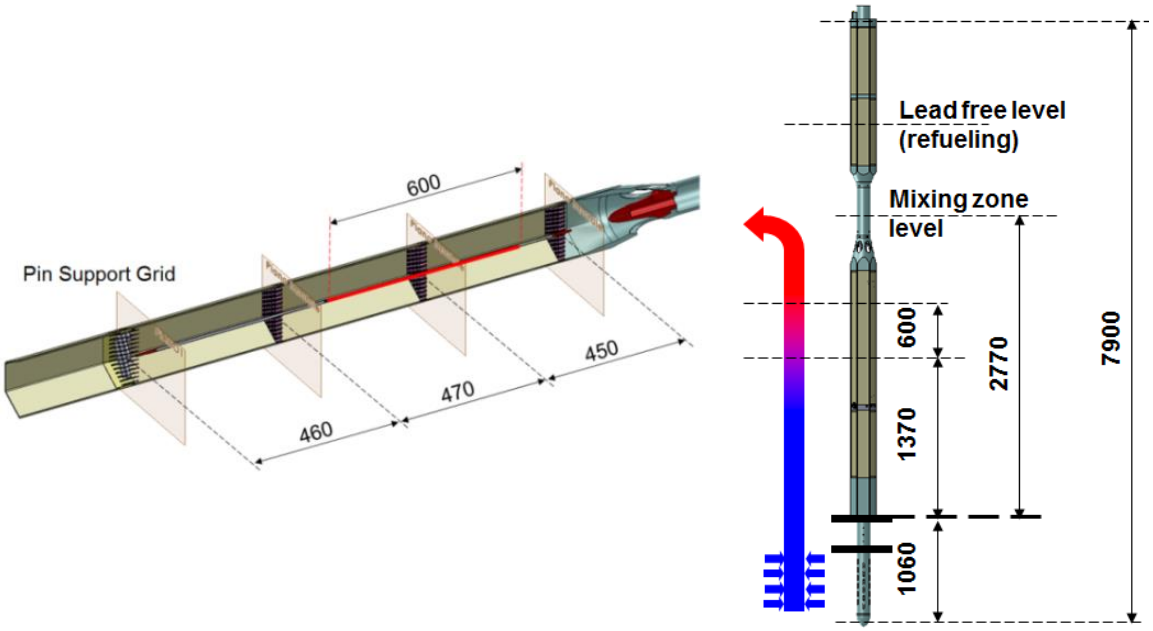

Figure 12. Fuel assembly geometry (lengths are expressed in mm).

As far as the distributed losses within the coolant channels are concerned, they have been preliminarily estimated adopting the Mc-Adams correlation (Todreas and Kazimi, 2012) for the Fanning friction factor. On the other hand, the modelling of the form losses has turned out to be difficult since the dimensional specifications concerning the spacers have not been assessed yet. At this point, since the total pressure losses are specified in the core design and the distributed

ones have been evaluated, it has been easy to obtain the contribution of the form losses, representing the influence of the spacers in the core thermal-hydraulics by using the dedicated component *Orifice*, which allows to implement a suitable hydraulic resistance.

Component	Description
Sup D	Upper region of dummy elements
Active_Dummy	Region of dummy elements corresponding to the active zone of fuel assemblies
Inf D	Lower region of dummy elements
Empty D	Empty region of dummy elements
Orifice	Form pressure drop which allow to achieve the real pressure field
Sup FA	Upper region of fuel assemblies
LeadTube	Active region of fuel assemblies
Inf FA	Lower region of fuel assemblies
Empty	Empty region of fuel assemblies

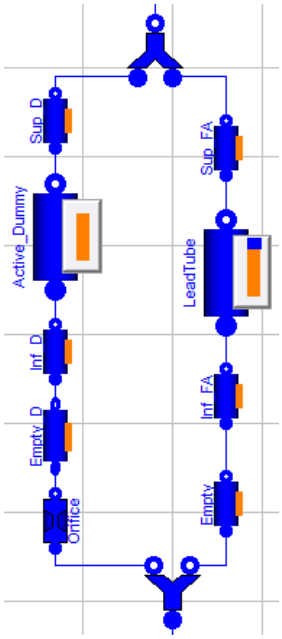

Figure 13. Detailed view of ALFRED core: representation of coolant channels.

All the several core subsystems have been eventually connected. In particular, the mutual influences between neutronics and thermal-hydraulics have been taken into account by means of the above mentioned feedback reactivity coefficients represented in the Modelica language through dedicated *connectors*. As shown in Figure 8, blue, grey and red connectors allow to carry the information about lead, cladding and fuel thermal behaviour in order to consider their influence on the neutronics.

2.2.2. Hot and cold pool

The coolant hot and cold pool models (named *Hot_pool* and *Cold_pool*) have been implemented by employing a component describing a free-surface cylindrical lead tank (responsible for most of the large thermal inertia characterizing the overall system), on which mass and energy

balances have been taken, assuming that no heat transfer occurs, except through the inlet and outlet boundaries.

2.2.3. Hot and cold legs

In order to represent transport phenomena, simple one-phase *LeadTube* components have been employed (named *Hot_leg* and *Cold_leg*). One-dimensional flow models have been implemented, neglecting thermal dispersion, to properly consider the time delays due to transport phenomena between the core and the SG, and between the SG and the cold pool.

2.2.4. Pumps

As far as the primary and secondary pumps are concerned, ideal flow rate regulators have been employed.

2.2.5. Steam generator

Due to its non-conventional bayonet-tube design, an effort has been spent to set up a specific component representing the ALFRED SG (Figure 14). A simplified description has been adopted, based on a one-dimensional description of the actual geometry, which has been reproduced by means of different tube models connected together. In this way, the advantage of reusability of the Modelica models has been exploited. Indeed, the same tube, based on a certain set of equations, can be employed in different contexts and then extended through *inheritance* by adding further equations. After entering the SG, water flows down in the slave tube (see Appendix A) and there is no heat exchange neither thermal dispersion, thanks to the effective insulation provided. Thus, water conditions at the SG inlet and at the bottom of the tube are the same. For this reason, this first part has been neglected and the feedwater has been simulated to flow directly in a counter-current configuration, exchanging thermal power with the external lead. The component geometry has been substituted with concentric tube bundles in a counter-current flow configuration where the pressure drops are concentrated at the bayonet bottom (i.e., where the fluid flow reverses). A turbulent, lumped pressure drop model has been assumed, proportional to the kinetic pressure.

As far as the water side is concerned, a tube allowing to describe a two-phase fluid has been selected, adopting averaged densities in the neighbourhood of phase changes so as to avoid non-physical simulation artefacts due to phase change discontinuities at the model nodes. A two-phase homogeneous model (i.e., with the same velocity for the liquid and vapour phases) has been adopted.

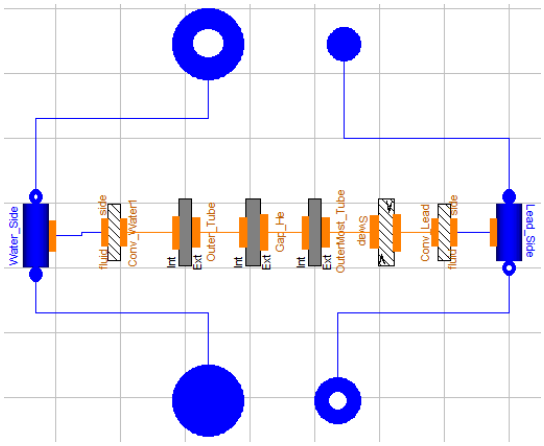

Component	Description
Water_Side	Tube model that describes the water flowing.
Conv_Water	Component that describes the convective heat transfer on water side.
Outer_tube, Gap_He, Outermost_tube	Components that allows for the conduction phenomena within the different interfaces.
Swap	Component that allows to reproduce the counter-current configuration.
Conv_Lead	Component that describes the convective heat transfer on lead side.
Lead_Side	Tube model that describes the lead flowing.

Figure 14. ALFRED SG object-oriented model.

Water-side convective heat transfer coefficients have been evaluated by implementing the Dittus-Boelter correlation for one-phase regions, and the Kandlikar correlation for the boiling region (Todreas and Kazimi, 2012). According to the latter correlation, the two-phase heat transfer coefficient, h_{TP}, is equal to the larger of $h_{TP,NBD}$ and $h_{TP,CBD}$, i.e., the two-phase heat transfer coefficients in the nucleate boiling dominant and convective boiling dominant regions, respectively. These coefficients are given by the following equations:

$$h_{TP,NBD} = 0.6683 Co^{-0.2} (1-x_v)^{0.8} f(Fr_{LO}) h_{LO} + 1058.0 Bo^{0.7} (1-x_v)^{0.8} F_{Fl} h_{LO} \quad (29)$$

$$h_{TP,CBD} = 1.136 Co^{-0.9} (1-x_v)^{0.8} f(Fr_{LO}) h_{LO} + 667.2 Bo^{0.7} (1-x_v)^{0.8} F_{Fl} h_{LO} \quad (30)$$

where $Co = (d_L/d_V)^{0.5}[(1- x_v)/ x_v]^{0.8}$ and $Bo = q''/(w \cdot i_{LG})$ are the convection and boiling numbers, respectively. F_{Fl} is the fluid-surface parameter that incorporates the effect of surface and fluid properties, and allows to take into account differences in nucleating characteristics. h_{LO} is the single-phase heat transfer coefficient with all flow as liquid. The function $f(Fr_{LO})$ is a Froude number with all flow as liquid. This parameter addresses the stratified flow region.

On the lead side, the component describing the behaviour of a single-phase fluid, previously used for the core model, has been adopted. Convective heat transfer coefficients have been evaluated by implementing the Ibragimov-Subbotin-Ushakov correlation as well. The multiple wall interfaces have been modelled by adopting different conductive-exchange elements, in which thermal resistance is computed according to the formulation of Fourier equation in cylindrical coordinates, while the heat capacity is lumped in the middle of the tube thickness. Dedicated components have been implemented to represent each interface constitutive layer (i.e., insulating layer, outer tube, helium gap, outermost tube). Besides, the *HeatTransfer* component has been used to evaluate the convective heat exchange on both water and lead sides, a *Swap* component has been adopted to allow for the counter-current configuration. In this way, temperature and flux vectors on one side are swapped with respect to the ones on the other side. Furthermore, only one SG with a suitably rescaled number of tubes guaranteeing a thermal power of 300 MW_{th} (instead of the actual eight 37.5 MW_{th} SGs) has been considered.

2.2.6. Outlet header

The steam coming out from the SG is suitably collected in a *header*, i.e., a well-mixed chamber having no pressure drop and no energy exchange with the environment that allows to dampen any pressure transient, limiting the impact on the conditions of the steam that flows into the turbine.

2.2.7. Attemperator

An attemperator has been foreseen between the outlet header and turbine, i.e., a reduced water mass flow rate at saturation conditions that is added to the steam flow. In this way, it is possible to promptly limit the steam temperature at the turbine inlet keeping this variable of interest as close as possible to its nominal value (450°C).

2.2.8. Turbine unit

Particular attention has been paid to this component, which is fundamental to properly take into account the electrical power provided to the grid, and constitutes a crucial parameter in a control perspective. The component selected for the turbine model describes a simplified steam turbine unit in which a fraction of the available enthalpy drop is disposed by the High Pressure (HP)

stage, whereas the remaining part by the Low Pressure (LP) one, with different time constants. A valve governs the overheated steam mass flow rate passing through the turbine. By adopting a simplified approach, choke flow conditions have been imposed. If the ratio of upstream pressure to downstream pressure is higher than the critical ratio ($x_c \approx 0.5$), in the section of maximum damping of the fluid vein a sonic shock wave is produced (Dolezal and Varcop, 1970). In this way, the inlet steam mass flow rate does not depend on the downstream pressure, namely:

$$\frac{p_{up} - p_{down}}{p_{up}} > x_c \quad \Rightarrow \quad w_v = A_v \lambda_c \sqrt{d_v(p) p} \tag{31}$$

Given that, it is possible to adopt the following approximation for the superheated steam:

$$d_v(p) p \propto p^2 \tag{32}$$

It follows that:

$$w_v \cong k_v p \tag{33}$$

Accordingly, the steam mass flow rate is regarded proportional to the inlet pressure and governed by operating the turbine admission valve (system input), not by throttling (i.e., no loss of thermodynamic efficiency occurs).

2.2.9. Bypass

After having passed through the SG, downstream of the temperature sensor, the steam mass flow rate can be subdivided into two ways (Figure 15). The former is a pipe that leads to the turbine, whereas the latter constitutes a bypass that directly leads to the condenser. This "alternative way" performs a very important function in particular operative conditions of the secondary side, when the reactor is operating at very low power levels, such as during the start-up phase. Indeed, when the thermal power from the primary circuit is not sufficient to ensure the steam nominal conditions, the flow is directly disposed to the condenser to avoid jeopardizing the integrity of the turbine, which cannot process an incoming fluid in such conditions. On the other hand, when the power level allows to obtain overheated steam, it is possible to let it flow to the turbine, while the bypass way is progressively closed.

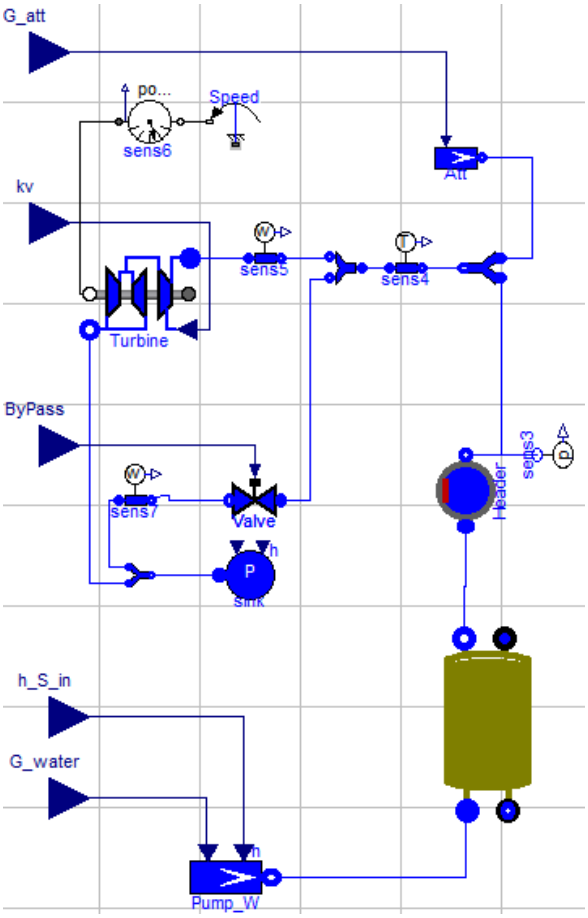

Figure 15. ALFRED reactor secondary side.

2.3 Free dynamics simulations

The reactor response to typical transient initiators has been investigated. In particular, three scenarios have been simulated, i.e., feedwater mass flow rate reduction, turbine admission valve coefficient variation, and Unprotected Transient of OverPower (UTOP), starting from nominal full power steady-state operating conditions. The tool developed in the present work allows to simulate a transient of 2500 s requiring a computational time of less than 30 seconds (2.20 GHz with 8 GB memory), hence turning out to be suitable for control-oriented purposes.

2.3.1 Reduction of the feedwater mass flow rate

The dynamic response of the system to a 20% step reduction of the feedwater mass flow rate has been investigated. This transient is particularly relevant in a control perspective since the feedwater mass flow rate may be considered as one of the most promising control variables for the regulation of the lead temperature in the cold pool. In particular, the latter has to be kept as close as possible to its nominal value (400°C). The main outcomes of this simulation scenario are the assessment of: (i) the dynamics of the transients, (ii) the influence of the feedwater mass flow rate on the lead temperature in the cold pool, i.e., quantify the temperature enhancement following the mass flow reduction; (iii) the compliance of the other variables of interest with the operational or safety limits; (iv) the coupling between the primary and the secondary circuit. Indeed, the feedwater mass flow variation affects also the secondary circuit, the steam generation and the electrical power production. Moreover, in the common nuclear control practice, after an enhancement of the power request by the electrical grid, the feedwater mass flow rate is usually enhanced to fulfil the loads demand. For these statements, it is relevant to investigate the system dynamic behaviour both for the primary and the secondary side, following a feedwater mass flow rate variation.

For the first 70 s, the only component affected by the perturbation is the SG itself, while in the second part of the transient SG and core are strongly coupled in virtue of reciprocal feedbacks. Since the other operating conditions are not modified (the turbine admission valve is not operated), the first consequences are a nearly step-wise pressure reduction in the SG (Figure 16a), a global worsening of the heat exchange conditions because of the combined effects of a

reduced mass flow rate and a narrower temperature difference between primary and secondary fluids. Therefore, an increase of the lead SG outlet temperature occurs (Figure 16b). When the hotter coolant begins to flow into the core, the lead average temperature increases (Figure 16c), inducing an insertion of negative reactivity (Figure 16d) that leads to a reduction of both core power and fuel temperature (Figure 16e-f). Nevertheless, the coolant core outlet temperature (Figure 16g) undergoes an increase, even if smaller than the inlet perturbation, and consequently hotter lead flows towards the SG inlet. The feedback to the secondary side is evident when examining the steam outlet temperature evolution (Figure 16h). Indeed, it rises almost instantaneously after the perturbation, and, when the core power starts decreasing, it continues increasing but exhibiting a smaller and smaller gradient, consistently with the progressive thermal power reduction, to the final steady-state condition. From the free dynamics analysis, it is possible to assess the time constants characterizing this plant which are key parameters for the development of the reactor control. In addition, relevant outcomes related to the control action necessary to satisfy the operational constraint are needed. In particular, a strong control action has to be carried out in order to keep the SG pressure as close as possible to its nominal value (180 bar) in order to avoid depressurization. The same attention has to be paid for the steam temperature since hotter (or colder) vapour condition can jeopardize the turbine stages.

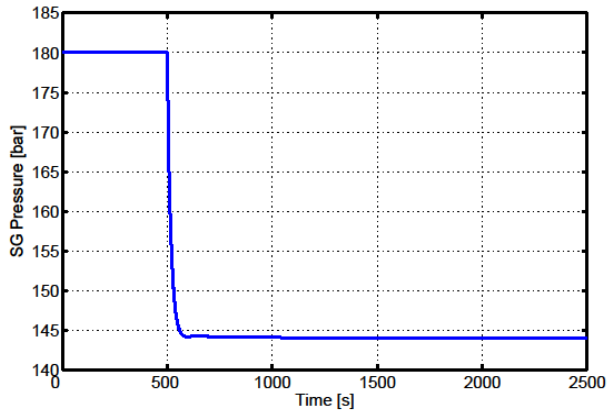

(a)

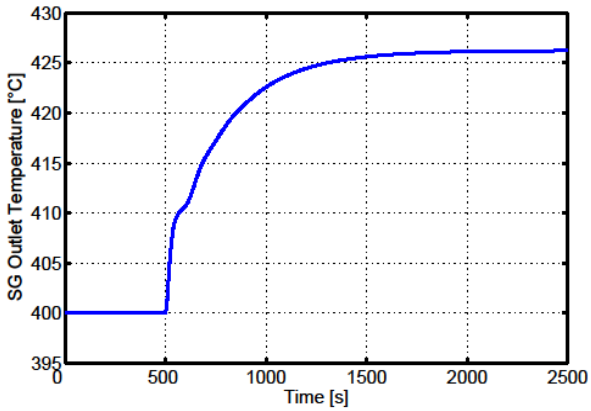

(b)

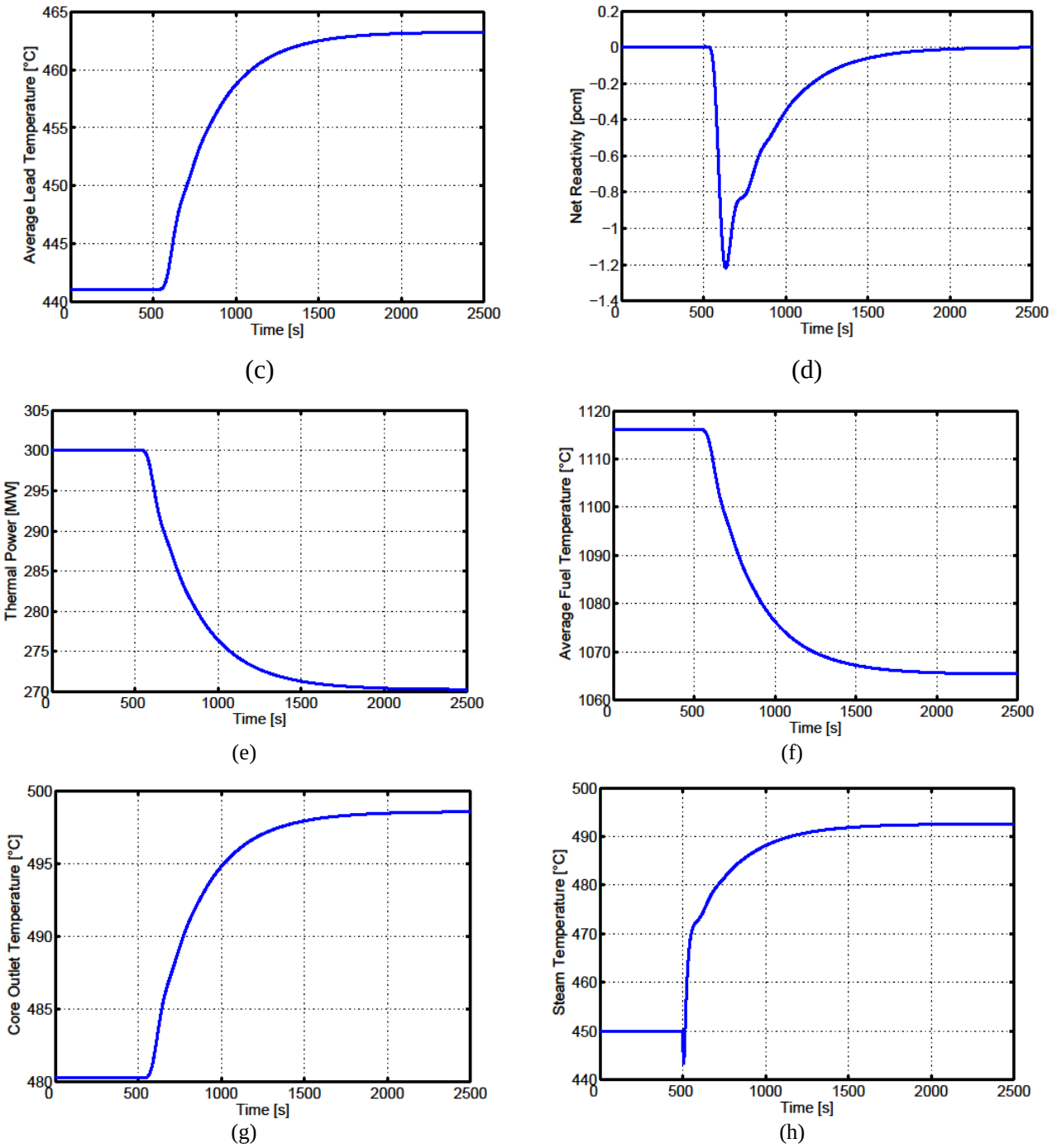

Figure 16. Variables evolution after a feedwater mass flow rate reduction: (a) SG pressure variation; (b) lead SG outlet temperature variation; (c) average lead temperature variation; (d) net reactivity variation; (e) core thermal power variation; (f) average fuel temperature variation; (g) core outlet temperature variation; (h) steam temperature variation.

2.3.2. Variation of the turbine admission valve coefficient

In order to study the system behaviour after a change of the grid request, the system response after a 10% reduction of the turbine admission valve flow coefficient has been simulated. This is another fundamental transient for the control design since it allows evaluating the possibility of performing load-frequency regulation according to the grid demands by adopting this kind of reactor. In particular, in case of power decrease, the power regulation is achieved by closing the turbine admission valve. In this way, a lower steam mass flow rate circulates in the turbine and a lower mechanical power is available to the alternator. As far as the SGs are concerned, the pressure increase following the valve closing is compensated by a simultaneous control action performed both on feedwater mass flow rate and control rods in order to balance the power produced. This transient is relevant in the control strategy definition and characterization because of ALFRED is meant to be employed as a NPP connected to the electrical grid.

The first consequence of the performed perturbation is an instantaneous pressure rise within the SG (Figure 17a) since in the simulated transient a coordinated control strategy is not carried out. Because of the secondary fluid sudden compression, the temperature difference between primary and secondary fluids decreases and a lower power transfer occurs, inducing a lead temperature enhancement at the SG outlet (Figure 17b). The ensuing negative reactivity insertion (Figure 17c) determines a core power reduction (Figure 17d). As to the coolant core outlet temperature (Figure 17e), an increase is observed even though slighter than the one at the core inlet.

It is worthwhile discussing the behaviour of the steam temperature (Figure 17f). In the first part of the transient, its evolution is characterized by the typical dynamics of a stand-alone SG. The initial sudden rise is due to the fact that the turbine admission variation causes a mass flow rate reduction and, at constant thermal power exchanged, the steam gets hotter and hotter. Nevertheless, the overall tube is immediately affected by the pressure change and by the consequent saturation temperature increase, and therefore the overheated region within the tube gets shorter and the steam temperature decreases. After 70 s, the SG starts perceiving the effects ensuing from the core evolution and then, according to the core outlet lead temperature, the steam temperature increases until the system settles at a higher new steady-state value. The main outcome of this simulation is that, in virtue of the values assumed by the reactivity feedback

coefficients, the ALFRED reactor response, following the turbine admission valve variation can be considered similar to the PWRs' ("reactor follows turbine"), though the characteristic time constant are definitely longer. It is worthwhile to remind that, even this similarity with the classic and well-known reactor concept, the control scheme developed for the PWRs cannot be applied "as it is" to the LFR due to the different constraints to be fulfilled (e.g. the lead temperature in the cold pool has to be kept as close as possible to 400°C).

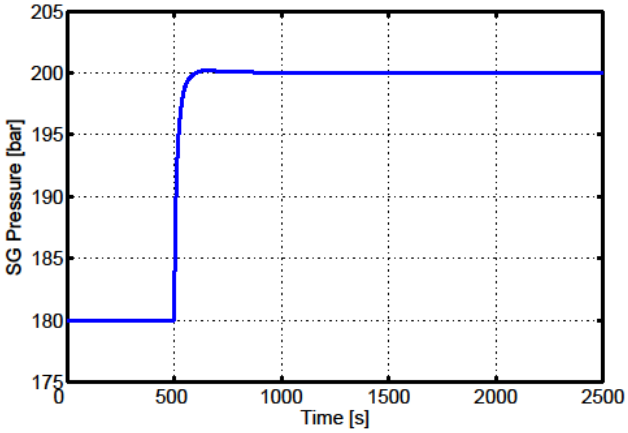

(a)

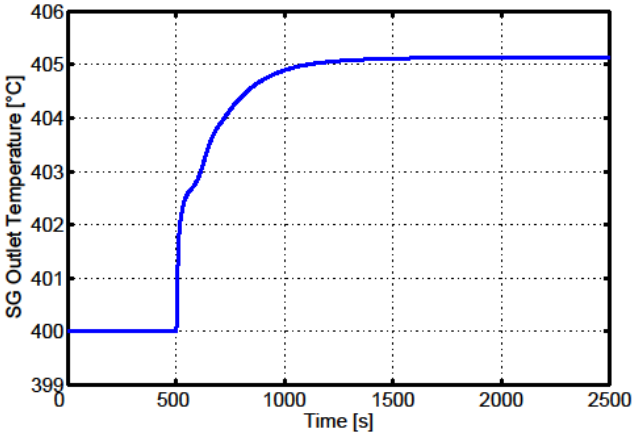

(b)

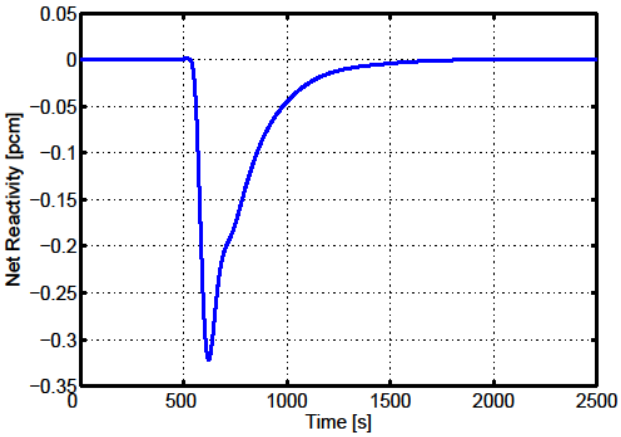

(c)

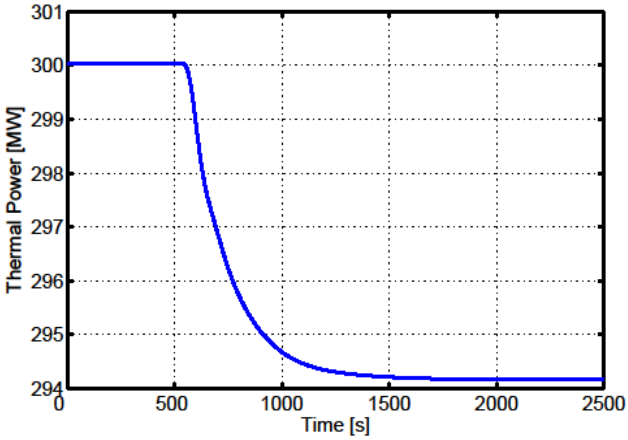

(d)

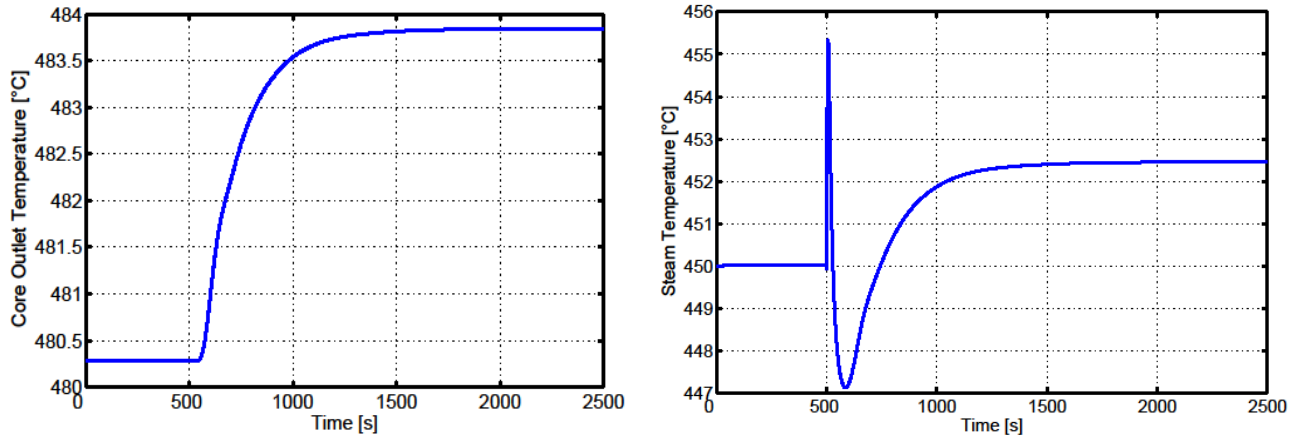

(e) (f)

Figure 17. Variables evolution after a variation of the turbine admission valve coefficient: (a) SG pressure variation; (b) lead SG outlet temperature variation; (c) net reactivity variation; (d) core thermal power variation; (e) core outlet temperature; (f) steam temperature variation.

2.3.3. Unprotected Transient of Over Power (UTOP)

An extraction of control rods corresponding to a 20 pcm step reactivity variation (Figure 18a) has been simulated. This is an interesting operational transient to be evaluated since it involves the dynamics associated to the handling of the control rods, and how this kind of perturbation has effect on the rest of the plant. This core-driven simulation determines an immediate feedback to the SG due to the coolant core outlet temperature enhancement. Thanks to the presence of the pool, the action of the SG on the core, consisting in an increase of the coolant core inlet temperature, is delayed and softened.

For the first part of transient, the behaviour of the system is the same as if a stand-alone core simulation were performed. Indeed, after the step-wise insertion of reactivity given by control rods the power suddenly increases exhibiting the typical prompt jump behaviour and, after a small decrease, starts reaching the steady-state (Figure 18b). The reactivity insertion in the core affects the SG as a temperature enhancement of the lead coming from the core (Figure 18c). As a direct consequence of the improved heat exchange conditions due to the hotter primary fluid, the steam temperature increases (Figure 18d). The abrupt change of the steam density determines a perturbation in the SG pressure (Figure 18e), which ends when the primary circuit reaches a new equilibrium condition. The higher thermal power level promotes an enhancement of the lead SG outlet temperature (Figure 18f). As far as the core behaviour is concerned, the MOX-based fuel

elements, because of the low thermal conductivity, cause a stepwise increase of fuel temperature and, consequently, of the coolant average temperatures (Figure 18g-h), after the reactivity insertion. This response produces an immediate feedback on the system due to the Doppler effect and to lead density contribution, which cause an abrupt inversion of the reactivity evolution that quickly gets back to zero.

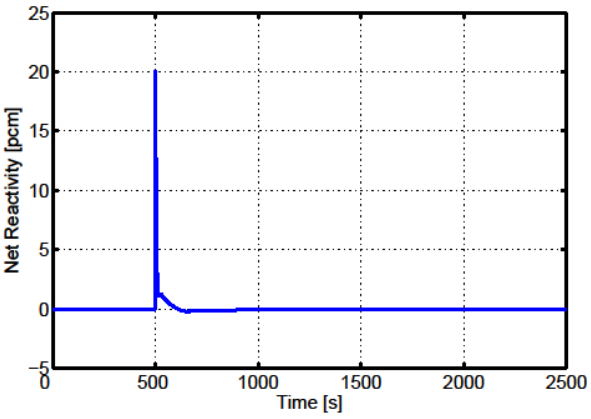

(a)

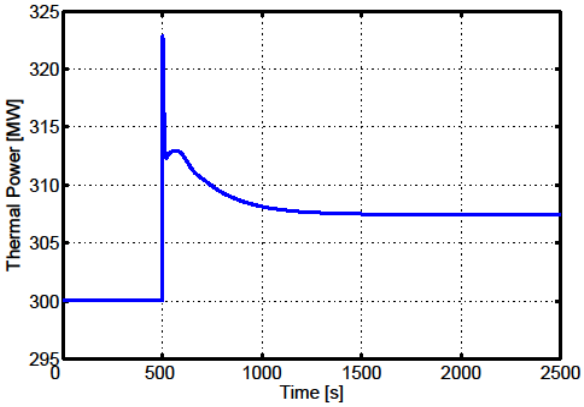

(b)

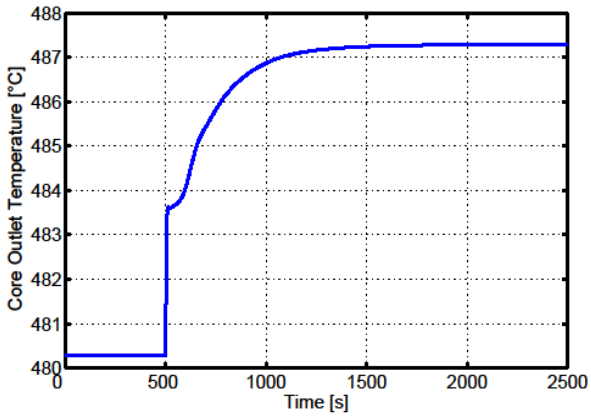

(c)

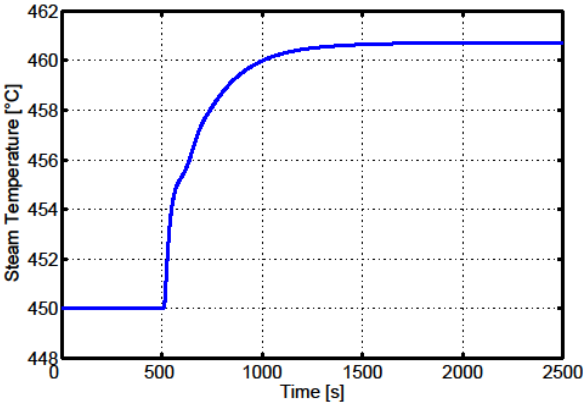

(d)

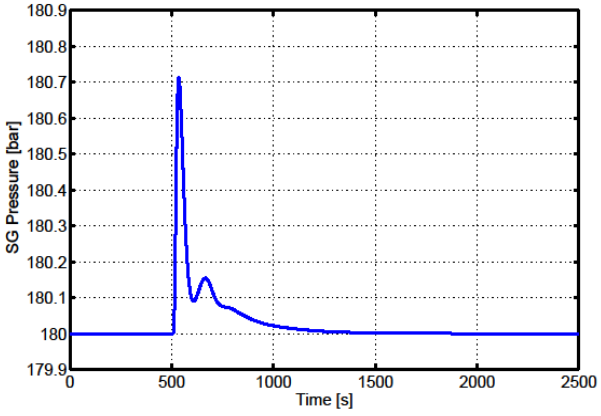

(e)

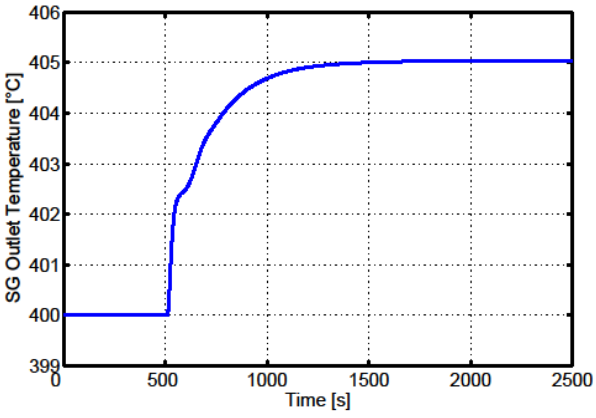

(f)

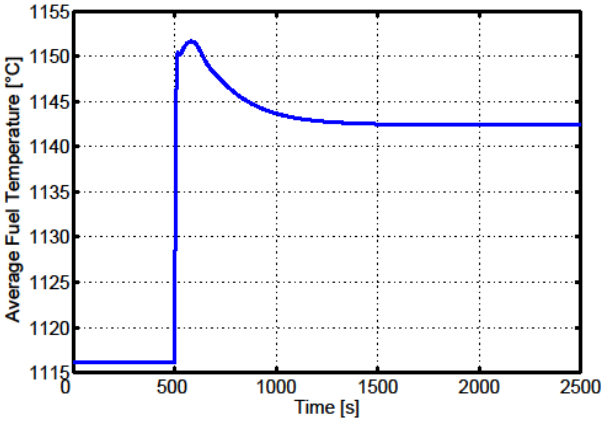

(g)

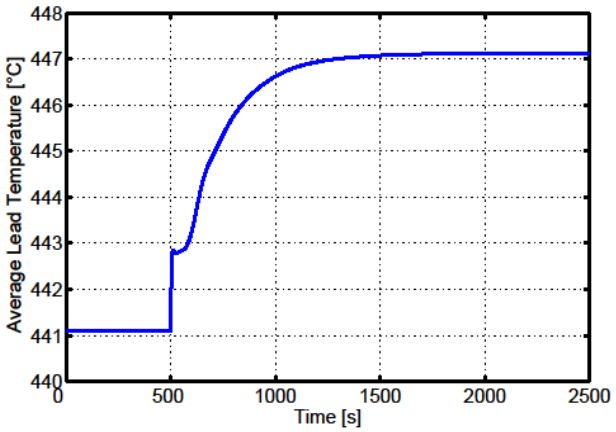

(h)

Figure 18. Variables evolution after a step reactivity variation: (a) net reactivity variation; (b) core thermal power variation; (c) core outlet temperature variation; (d) steam temperature variation; (e) SG pressure variation; (f) lead SG outlet temperature variation; (g) average fuel temperature variation; (h) average lead temperature variation.

2.4 Stability analysis verification

The object-oriented model has been exploited also to verify the outcomes of the stability analysis since the latter is based on a lumped approach with constant parameter. In this way, the model can be easily linearized and the sensitivity analysis on the lead coefficient and the power can be performed. On the other hand, the results are affected by these assumptions. In order to confirm the conclusions of the stability analysis some transients have been performed with the more accurate object-oriented model of the ALFRED reactor.

2.4.1 Stand alone core

As for the stand alone core, the results of the stability analysis indicates that a coolant density coefficient between 12 and 13 pcm/K makes the reactor unstable. Accordingly two simulations with the object-oriented model have been performed with α_L = 9 pcm/K and α_L = 13 pcm/K, respectively. In particular, a reactivity insertion of 0.1 $ is studied. In the first case, the results (Figure 19) confirms the stability analysis outcomes since the reactor power reaches a new stable level. On the other hand, with α_L = 13 pcm/K, the simulation stop 50 s after the reactivity insertion since the power reaches high level, the reactivity approaches the dollar threshold and the fuel is close to the melting point (Figure 20).

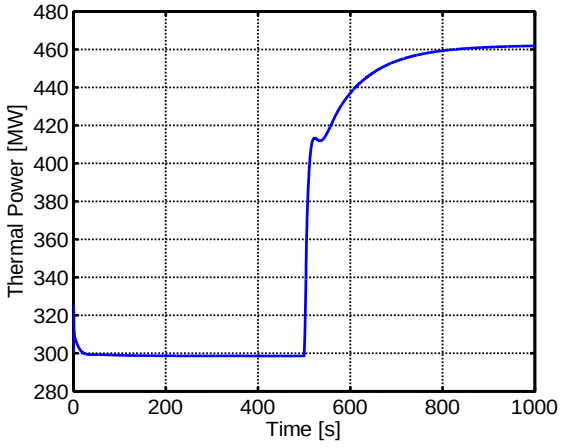

(a)

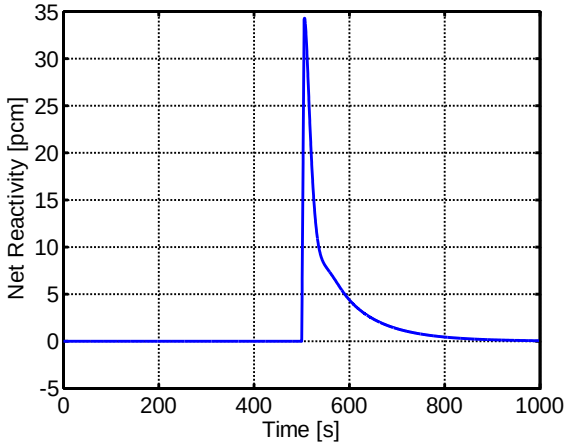

(b)

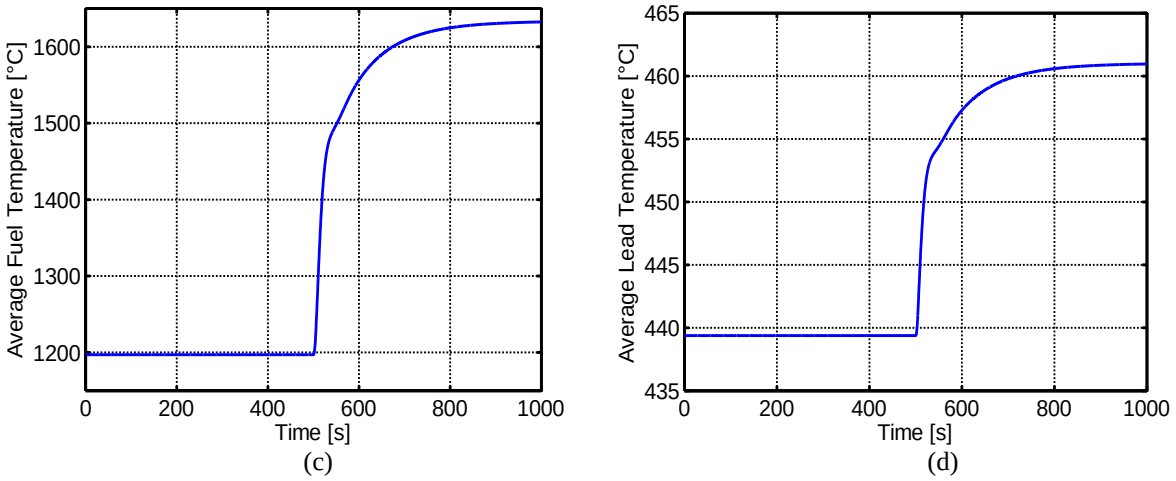

Figure 19. Variables evolution after a step reactivity variation, stand alone core with α_L = 9 pcm/K: (a) core thermal power variation; (b) net reactivity variation; (c) average fuel temperature variation; (d) average lead temperature variation.

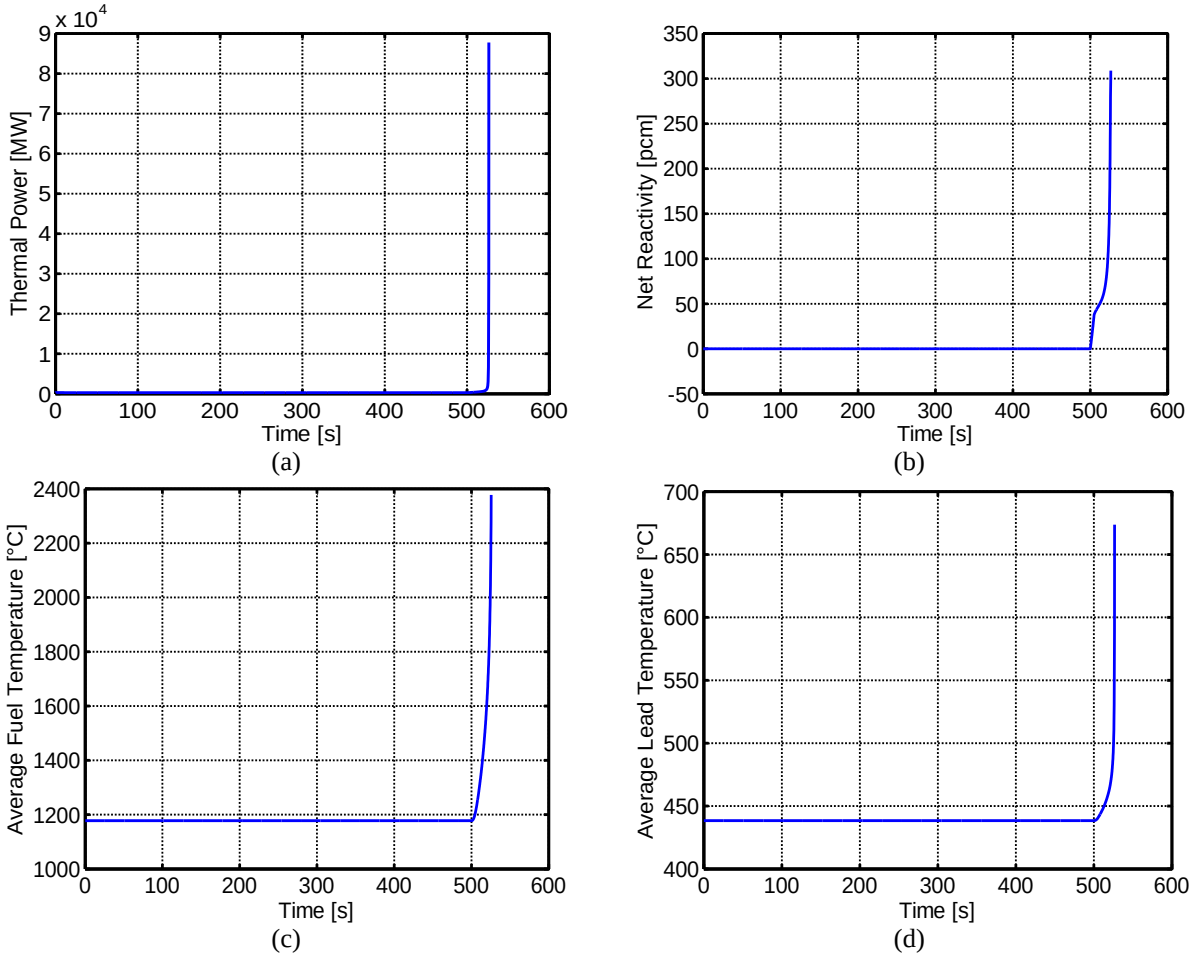

Figure 20. Variables evolution after a step reactivity variation, stand alone core with α_L = 13 pcm/K: (a) core thermal power variation; (b) net reactivity variation; (c) average fuel temperature variation; (d) average lead temperature variation.

As for the power dependency is concerned, the stability analysis points out that the system at nominal power becomes unstable for the lowest lead density coefficient. This trend is mainly due to the amplified feedback effects at higher power. This result has been confirmed performing a reactivity insertion simulation at reduced power level with α_L = 13 pcm/K. In the previous simulation, the system turned out to be unstable with this lead density reactivity coefficient at nominal power level. On the other hand, if we start with a reduced power level, the results indicate that the system is no more unstable (Figure 21) as the stability analysis predicts. In particular, if the power reactor is settled at a lower level respect to the nominal one, an higher value of the α_L is need to make the reactor unstable.

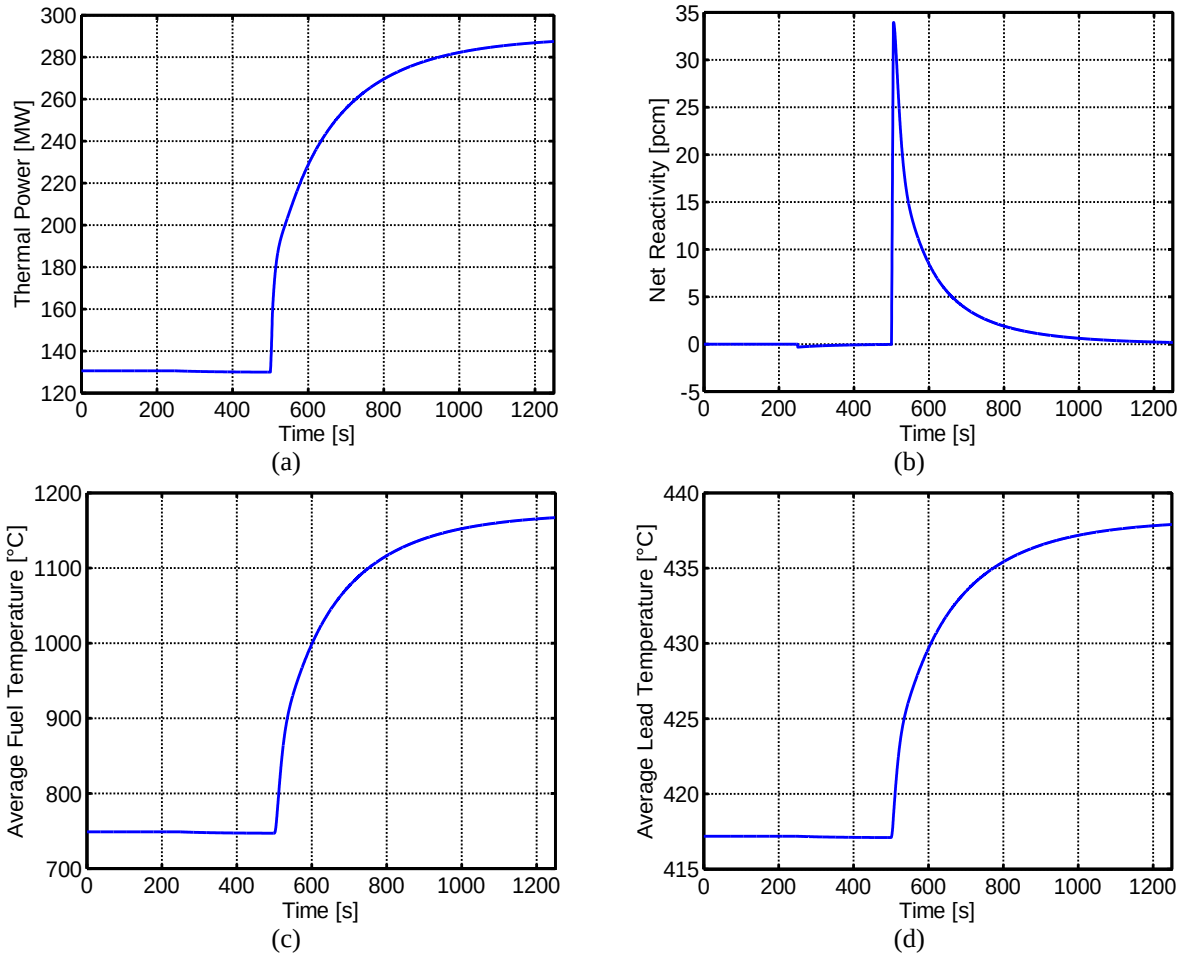

Figure 21. Variables evolution after a step reactivity variation, stand alone core with α_L = 13 pcm/K at reduced power level: (a) core thermal power variation; (b) net reactivity variation; (c) average fuel temperature variation; (d) average lead temperature variation.

2.4.2. Primary loop

As for the primary loop, the results of the stability analysis indicates that a coolant density coefficient between 6 and 7 pcm/K makes the reactor unstable. Accordingly two simulations with the object-oriented model have been performed with α_L = 2 pcm/K and α_L = 7 pcm/K, respectively. In particular, a reactivity insertion of 0.1 $ is studied. In the first case, the results (Figure 22) confirms the stability analysis outcomes since the reactor power reaches a new stable level. On the other hand, with α_L = 7 pcm/K, the simulation stop since the power reaches high level and the fuel is close to the melting point (Figure 23).

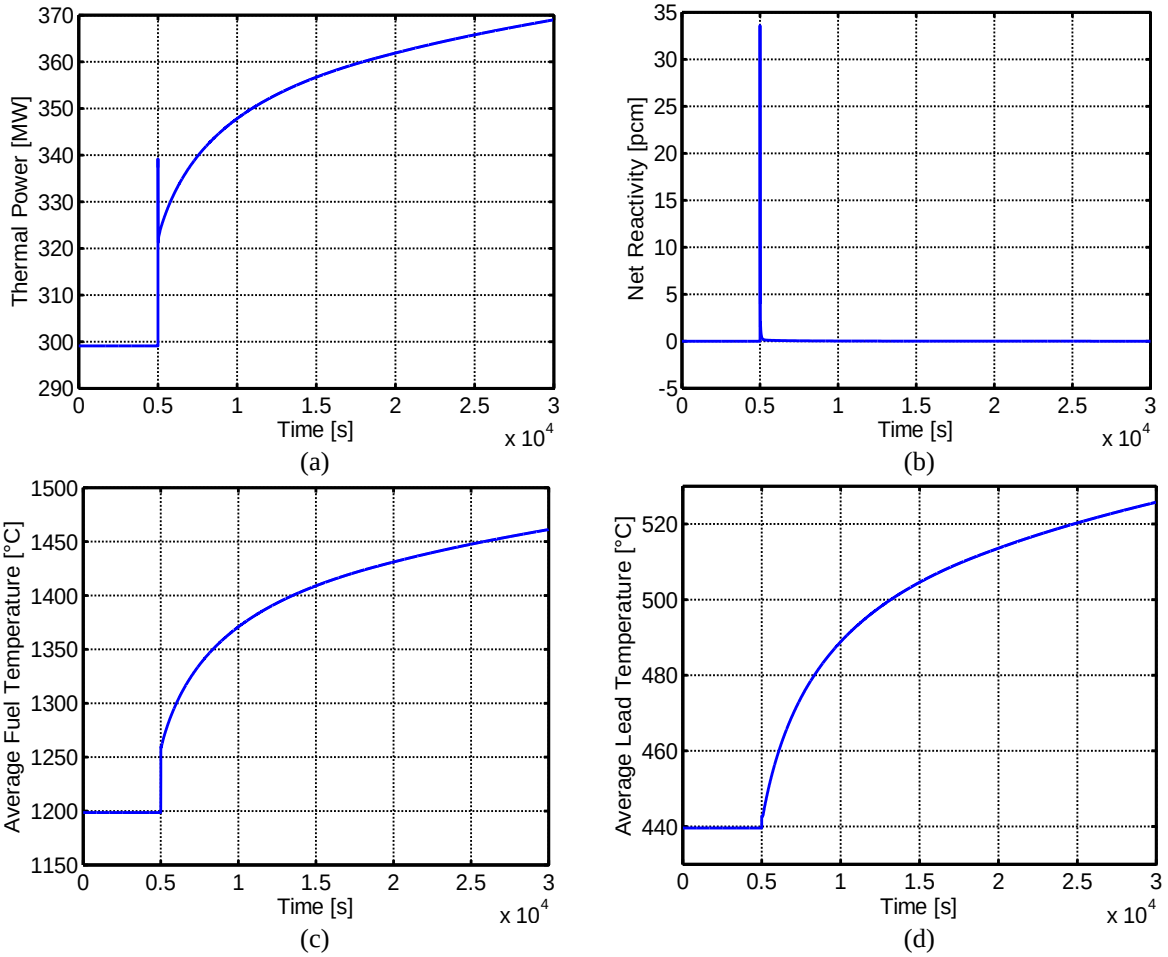

Figure 22. Variables evolution after a step reactivity variation, primary loop with α_L = 2 pcm/K: (a) core thermal power variation; (b) net reactivity variation; (c) average fuel temperature variation; (d) average lead temperature variation.

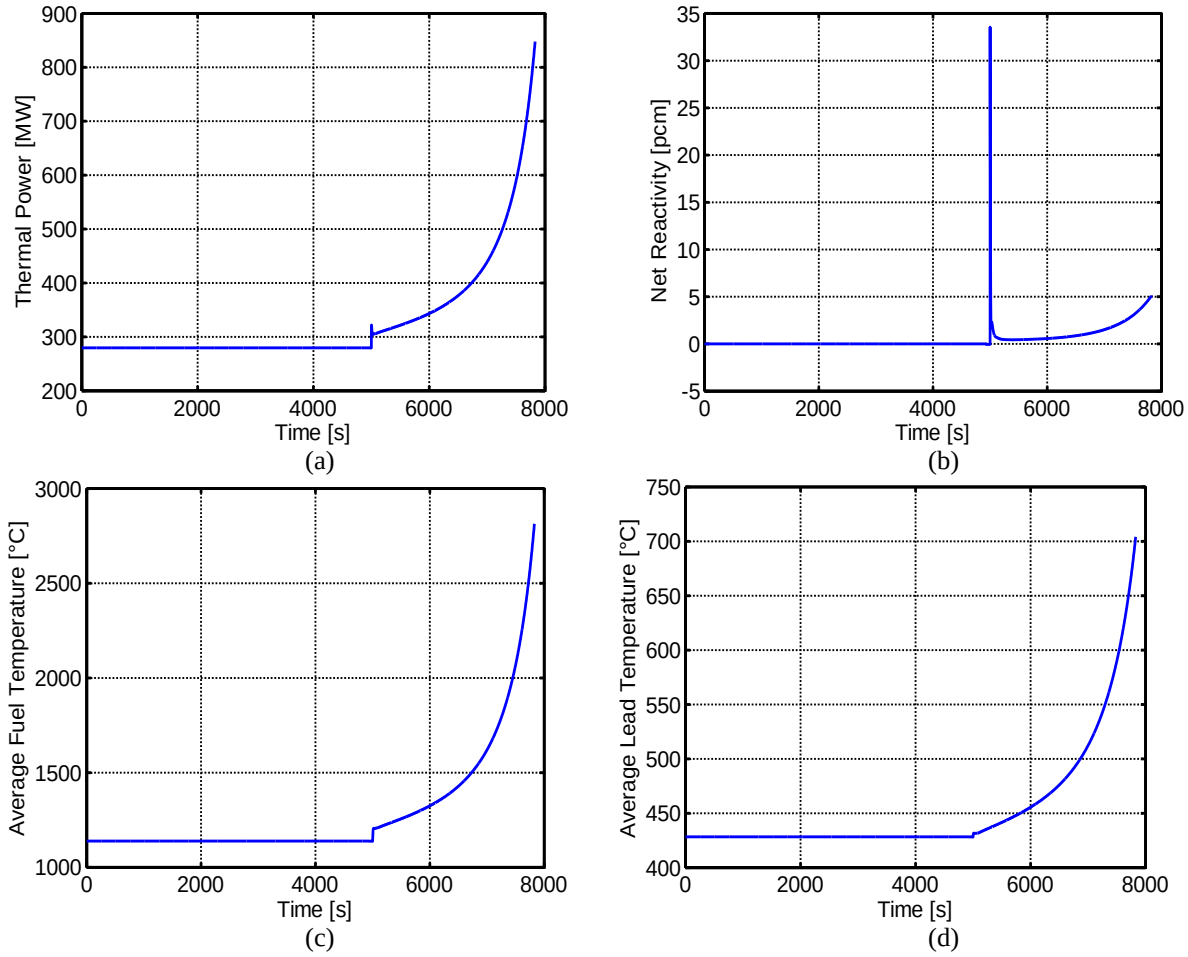

Figure 23. Variables evolution after a step reactivity variation, primary loop with α_L = 7 pcm/K: (a) core thermal power variation; (b) net reactivity variation; (c) average fuel temperature variation; (d) average lead temperature variation.

As for the power dependency is concerned, also for the primary loop, the stability analysis points out that the system at nominal power becomes unstable for the lowest lead density coefficient. This result has been confirmed performing a reactivity insertion simulation at reduced power level with α_L = 7 pcm/K. In the previous simulation, the system turned out to be unstable with this lead density reactivity coefficient at nominal power level. On the other hand, if we start with a reduced power level, the results indicate that the system is no more unstable (Figure 24) as the stability analysis predicts.

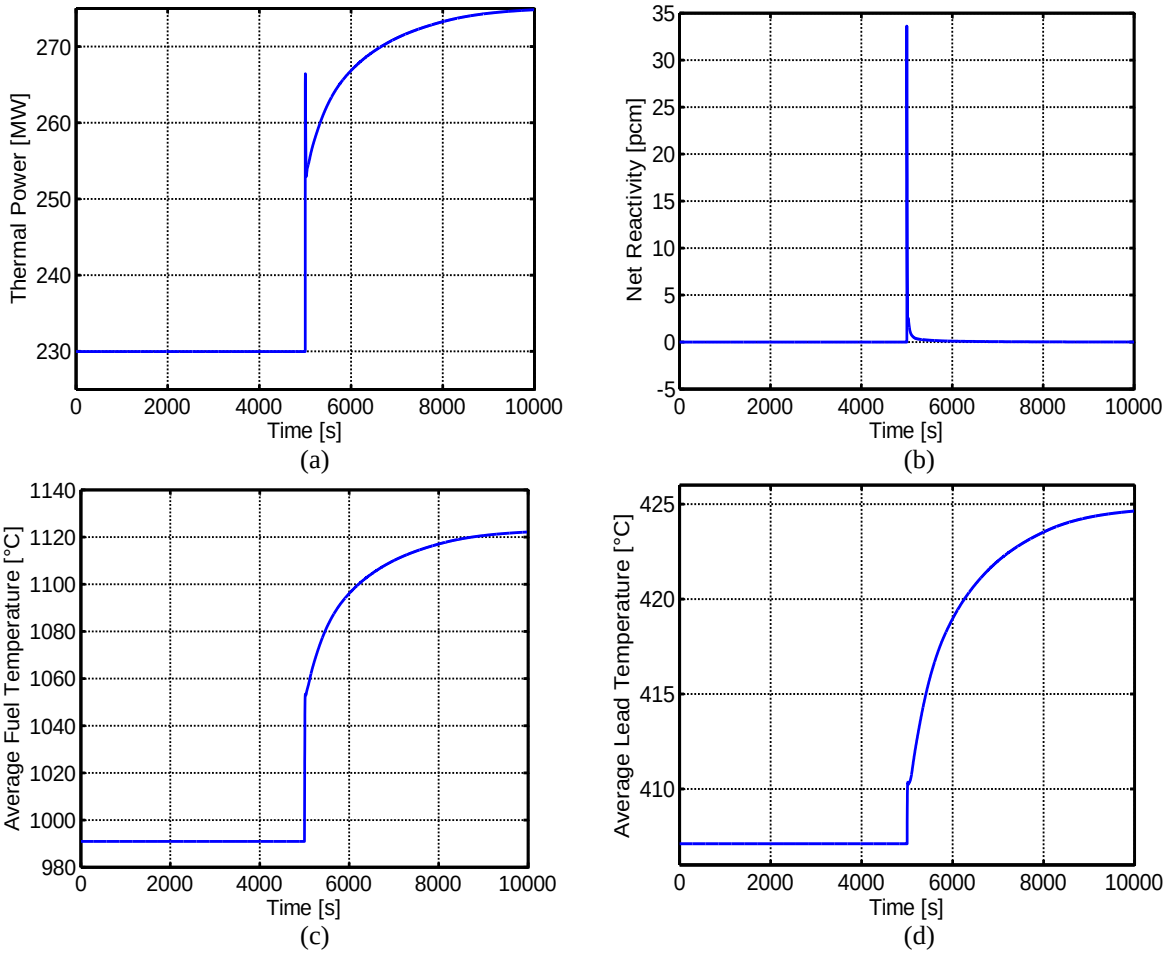

Figure 24. Variables evolution after a step reactivity variation, primary loop with α_L = 7 pcm/K at reduced power level: (a) core thermal power variation; (b) net reactivity variation; (c) average fuel temperature variation; (d) average lead temperature variation.

References

Alemberti, A., Frogheri, M., Mansani, L., 2013. The Lead fast reactor Demonstrator (ALFRED) and ELFR design. Proceedings of the International Conference on Fast Reactors and related Fuel Cycles: Safe Technologies and Sustainable Scenarios (FR 13), Paris, France, March 4-7, 2013.

Brenan, K.E., Campbell, S.L., Petzold, L.R., 1989. Numerical solution of initial-value problems in differential algebraic equations. North-Holland Ed.

Cammi, A., Casella, F., Ricotti, M.E., Schiavo, F., 2005. Object-Oriented Modelling, Simulation and Control of IRIS Nuclear Power Plant with Modelica. Proceedings of the 4th International Modelica Conference, Hamburg, Germany, March 7-8, 2005.

Cammi, A., Luzzi, L., 2008. Innovative Techniques for the Simulation and Control of Nuclear Power Plants. In: Durelle, V.B., Ed., Nuclear Energy Research Progress. Nova Science Publishers, Inc., Hauppauge, NY.

Casella, F., Leva, A., 2006. Modeling of thermo-hydraulic power generation processes using Modelica. Mathematical and Computer Modeling of Dynamical Systems, 12, 1, 19–33.

Cheng, X., Tak, N.-i., 2006. Investigation on Turbulent Heat Transfer to Lead-Bismuth Eutectic Flows in Circular Tubes for Nuclear Applications. Nuclear Engineering and Design, 236, 385–393.

Dolezal, R., Varcop, L., 1970. Process Dynamics: Automatic Control of Steam Generation Plant. Elsevier Science.

Elmqvist, H., Cellier, F.E., Otter, M., 1993. Object-Oriented Modeling of Hybrid Systems. Proceedings of the European Simulation Symposium (ESS'93), Delft, Netherlands, October 25-28, 1993.

Fritzson, P., 2004. Principles of Object-Oriented Modeling and Simulation with Modelica 2.1. Wiley-IEEE Press.

Fritzson, P., 2011. A cyber-physical modeling language and the OpenModelica environment. 7th International Wireless Communications and Mobile Computing Conference (IWCMC), Istanbul, Turkey, July 4-8, 2011.

Grasso, G., Petrovich, C., Mattioli, D., Artioli, C., Sciora, P., Gugiu, D., Bandini, G., Bubelis, E., and Mikityuk, K., 2014, "The Core Design of ALFRED, a Demonstrator for the European Lead-Cooled Reactors," Nucl. Eng. Des., 278, pp. 287–301.

Hetrick, D.L., 1971. Dynamics of Nuclear Reactors, University of Chicago Press, Chicago.

Kozlowski, T., Downar, T.J., 2007. PWR MOX/UO2 Core Transient Benchmark. Working Party on Scientific Issues of Reactor Systems. Nuclear Science NEA/NSC/DOC(2006)20, ISBN 92-64-02330-5.

Lyapunov, A.M., 1966. The Stability of Motion, Academic Press, New York and London.

Modelica, 2011. http://www.modelica.org.

OECD-NEA, 2007. Handbook on Lead-bismuth Eutectic Alloy and Lead Properties, Materials Compatibility. Thermal Hydraulics and Technologies, No. 6195.

Souyri, A., Bouskela, D., Pentori, B., Kerkar, N., 2006. Pressurized Water Reactor Modelling with Modelica. Proceedings of the 5th International Modelica Conference, Vienna, Austria, September 4-5, 2006.

The MathWorks, Inc. 2015.

Todreas, N., Kazimi, M.S., 2012. Nuclear Systems – Thermal Hydraulic Fundamentals. vol. 1, CRC Press, 2nd edition.

Waltar, A.E., Todd, D.R., and Tsvetkon, P.V., Editors, 2012. Fast Spectrum Reactors, Springer, New York (2012), ISBN 978-1-4419-9571-1.

Conclusions

In this report, two simulation tools for the assessment of the stability and the dynamics of the new ALFRED configuration have been developed. In this phase in which all the system specifications are reconsidered and thus are subject to modifications, tools providing the neutronics and thermal-hydraulics designers with fundamental feedbacks useful to improve or even finalize the system layout are extremely worthwhile. To this purpose, both a lumped-parameter and an object-oriented one-dimensional approach have been developed, the former devoted to the stability analysis and the latter aimed at studying the dynamics and verifying the outcomes of the previous one.

As for the lumped-parameter approach, the impact of fuel burn-up and the fundamental parameters on the system stability has been evaluated considering both a stand-alone core and a primary loop configuration. A crucial role is played by the coolant density coefficient that can be positive. As a major outcome, ALFRED has turned out to be inherently stable on the entire power range independently of both the fuel burn-up and the value of the coolant density coefficient, which should reach unrealistic high values (nearly 6 pcm K^{-1}) to make the reactor unstable.

The object-oriented plant simulator, incorporating also the BoP, consists of the following essential parts: core, steam generator, primary and secondary pumps, cold and hot legs, cold pool, turbine, and condenser. Both transient analyses and verification of the outcomes provided by the stability analysis have been performed. The outcomes of the free dynamics simulation confirm the coupling between core and SG, already outlined in the stability analysis. In addition, the border between the stability and instability zone have been confirmed by ad-hoc simulations.

As future developments, the simulation tools developed in this report are foreseen to be adopted to study and finalize the new ALFRED configuration.

(this page is intentionally left blank)

Appendix A: ALFRED reactor description

For the time being, the investigations are focused on the final configuration of the LEADER project, which can be considered the starting point of the new characterization. Nevertheless, in the further activities, the simulation tools developed in this report are foreseen to be adopted to study and finalize the new configuration.

ALFRED is a small-size (300 MWth) pool-type LFR. Its primary system current configuration (Alemberti et al., 2013) is depicted in Figure 25. All the major reactor primary system components, including core, primary pumps, and steam generators, are contained within the reactor vessel, being located in a large lead pool inside the reactor tank. The coolant flow coming from the cold pool enters the core and, once passed through the latter, is collected in a volume (hot collector) to be distributed to eight parallel pipes and delivered to as many steam generators. After leaving the SGs, the coolant enters the cold pool through the cold leg and returns to the core.

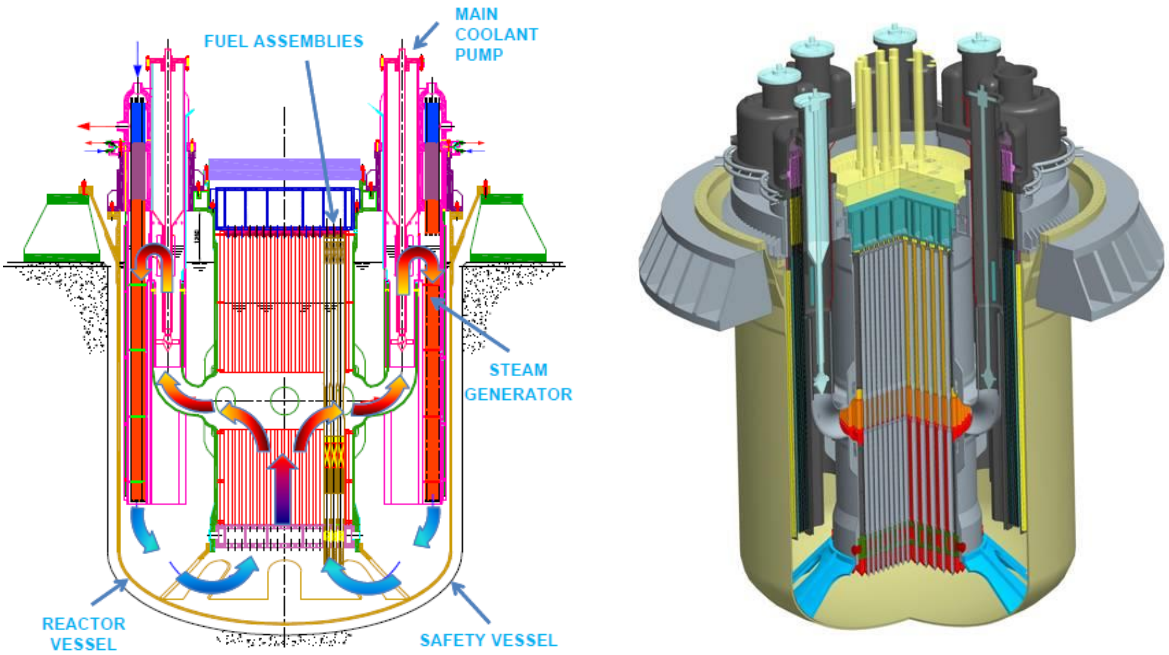

Figure 25. ALFRED nuclear power plant layout

The ALFRED core is composed by wrapped hexagonal Fuel Assemblies (FAs) with pins arranged on a triangular lattice (Figure 26). The 171 FAs are subdivided into two radial zones

with different plutonium fractions guaranteeing an effective power flattening, and surrounded by two rows of dummy elements (geometrically identical to the fuel assemblies but not producing thermal power) serving as reflector. Two different and independent control rods systems have been foreseen, namely, Control Rods (CRs) and Safety Rods (SRs). Power regulation and reactivity swing compensation during the cycle are performed by the former, while the simultaneous use of both is foreseen for scram purposes, assuring the required reliability for a safe shutdown (Grasso et al., 2013). In Table 2, the major preliminary nominal parameters employed as input data to implement the core model are presented.

Table 2. ALFRED core parameters (Grasso et al., 2013).

Parameter	Value		Unit
Core			
Thermal power	300		MW_{th}
Coolant mass flow rate	25984		kg s^{-1}
Total number of FAs	171		-
Pins per FA	127		-
Coolant inlet temperature, T_{in}	400		°C
Coolant outlet temperature, T_{out}	480		°C
Coolant flowing time (hot leg), τ_{HL}	10		s
Coolant flowing time (SG), τ_{SG}	10		s
Coolant flowing time (cold leg and pool), τ_{CL}	60		s
Fuel pin			
Cladding material	15-15-Ti		-
Fuel material	MOX		-
Cladding outer radius	$5.25 \cdot 10^{-3}$		m
Cladding inner radius	$4.65 \cdot 10^{-3}$		m
Pellet outer radius	$4.50 \cdot 10^{-3}$		m
Pellet inner radius	$1.00 \cdot 10^{-3}$		m
Active height	0.6		m
Reactivity and kinetic coefficients	*BoC*	*EoC*	
Doppler constant, K_D	-555	-566	pcm
Lead expansion coefficient[1], α_L	-0.271	-0.268	pcm K^{-1}
Axial clad expansion, α_{CZ}	0.037	0.039	pcm K^{-1}
Axial wrapper tube expansion, α_{WZ}	0.022	0.023	pcm K^{-1}
Radial clad expansion, α_{CR}	0.008	0.011	pcm K^{-1}
Radial wrapper tube expansion, α_{WR}	0.002	0.003	pcm K^{-1}
Axial fuel expansion[2] (linked case), α_{FZ}	-0.232	-0.242	pcm K^{-1}
Diagrid expansion[3], α_{Diag}	-0.147	-0.152	pcm K^{-1}
Pad expansion[3], α_{Pad}	-0.415	-0.430	pcm K^{-1}
Neutron generation time, Λ	$6.116 \cdot 10^{-7}$	$6.296 \cdot 10^{-7}$	s
Delayed neutron fraction, β	336	335	pcm

[1] Calculated for the whole height of the fissile sub-assemblies.
[2] In the stability analysis, α_Z refers to α_{FZ}.
[3] In the stability analysis, α_R refers to the sum of α_{Diag} and α_{Pad}.

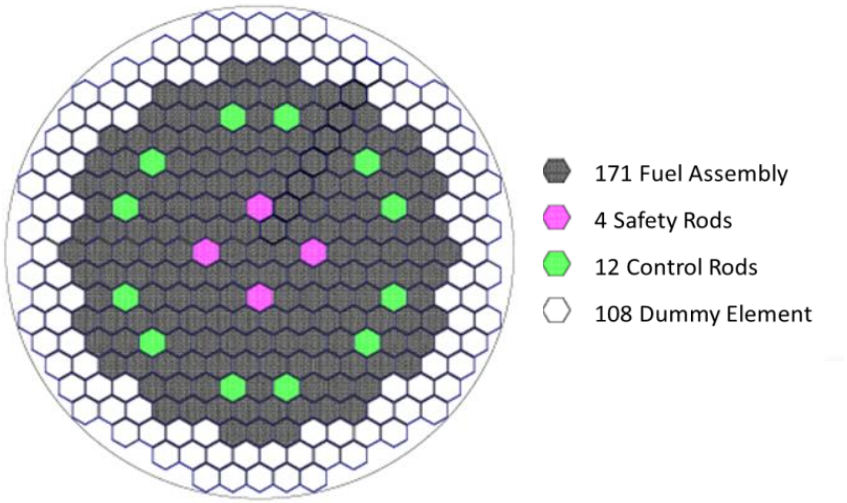

Figure 26. ALFRED core configuration.

Each of the eight SGs incorporated in ALFRED (Figure 27Figure 1) consists of a bundle of vertical bayonet tubes. Each one of these tubes is constituted by an external safety tube and an internal insulating layer (delimited by a slave tube), which is aimed at ensuring the production of superheated dry steam since the high temperature difference between the rising steam and the descending feedwater may promote steam condensation in the upper part of the SG without a proper insulation.

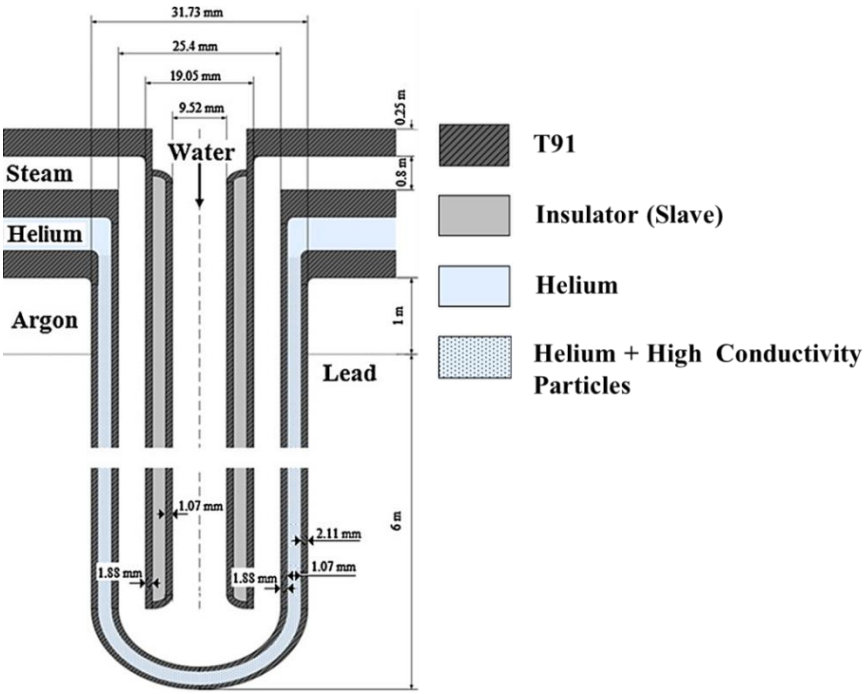

Figure 27. ALFRED bayonet tube SG configuration

The gap between the outermost and the outer bayonet tube provides mechanical decoupling between the components, and is filled with pressurized helium and high thermal conductivity particles to enhance the heat exchange capability (Alemberti et al., 2013). The feedwater from dedicated headers flows in the slave tube and, after reversing the motion at the bottom, rises along the annulus between inner and outer tubes. On the primary side, lead flows downwards axially along the outermost tube. In Table 3, the main SG parameters and specifications are listed.

Table 3. ALFRED SG major nominal parameters.

Parameter	**Value**		**Unit**
Single SG parameter			
Power	37.5		MW
Feedwater inlet temperature	335		°C
Steam outlet temperature	450		°C
Steam pressure	180		bar
Length of heat exchange	6		m
Number of tubes	510		-
	Outer diameter	*Thickness*	
Slave tube	$9.52 \cdot 10^{-3}$	$1.07 \cdot 10^{-3}$	m
Inner tube	$19.05 \cdot 10^{-3}$	$1.88 \cdot 10^{-3}$	m
Outer tube	$25.40 \cdot 10^{-3}$	$1.88 \cdot 10^{-3}$	m
Outermost tube	$31.75 \cdot 10^{-3}$	$2.11 \cdot 10^{-3}$	m